# Wavelength Dependent Photothermal Conversion Efficiency of Photosensitizers for Photothermal Therapy

by

Minahil Khan

A Dissertation Submitted to the
Graduate School of Sciences and Engineering
in Partial Fulfillment of the Requirements for
the Degree of

Master of Science

in

Materials Science and Engineering


January 24, 2021

# Wavelength Dependent Photothermal Conversion Efficiency of Photosensitizers for Photothermal Therapy

Koç University

Graduate School of Sciences and Engineering

This is to certify that I have examined this copy of a master's thesis by

**Minahil Khan**

and have found that it is complete and satisfactory in all respects,
and that any and all revisions required by the final
examining committee have been made.

Committee Members:

_____

Prof. ALPHAN SENNAROĞLU

_____

Prof. HAVVA YAĞCI ACAR

_____

Prof. M. BURÇİN ÜNLÜ

Date: _____

*[To my beloved mom, Saeeda Khalid]*

# ABSTRACT


**Wavelength Dependent Photothermal Conversion Efficiency of Photosensitizers for Photothermal Therapy**

**Minahil Khan**

**Materials Science and Engineering**

**January 24, 2021**

Today, cancer treatment is one of the most important research fields since it is the second most lethal disease worldwide. Among the current treatment methods that have strong potential for future cancer therapies is photothermal therapy (PTT). Nanoparticles have become popular photosensitizers for photothermal therapy (PTT), as they can be targeted to specific cancer tissues and deliver a chemotherapeutic drug, providing a multimodal therapeutic approach. Photothermal conversion efficiency of nanoparticles is critical in the assessment of their therapeutic use in PTT. In this thesis, we describe an accurate calorimetric method for the determination of the photothermal conversion efficiency of nanoparticles in solution. A tightly focused continuous wave laser beam was used to irradiate a cuvette containing a solution of silver sulfide-glutathione quantum dots ($Ag_2S$-GSH QDs), and the maximum steady-state temperature rise was measured with an infrared camera. The data were analyzed using two different photothermal conversion efficiencies, the intrinsic and external conversion efficiencies, to relate the induced heating power of the nanoparticles to the absorbed and incident optical powers, respectively. Measurements with a tunable $Ti^{3+}$:sapphire laser showed that the intrinsic photothermal conversion efficiency of $Ag_2S$GSH QDs exceeded 91% over the 720−810 nm wavelength range. The method was also used to analyze poly (acrylic acid)-coated superparamagnetic iron oxide nanoparticles (PAA/SPIONs), and the intrinsic photothermal conversion efficiency was determined to be 83.4% at 810 nm. At 640nm, PAA/SPIONs with 600 µg/ml of iron had intrinsic and extrinsic photothermal conversion efficiency of 76% and 63%, respectively. This approach is useful for the evaluation of various potential nanoparticles for photothermal therapy applications.

In additional *in vivo* experiments, $Ag_2S$-GSH Herceptin QDs were injected into mice grown with tumor SKBR3. Cisplatin was used as chemotherapeutic drug with the QDs.

Both Cisplatin and $Ag_2S$-GSH Herceptin QDs were injected subcutaneously into the mouse and investigated for different drug dozes of 10 mg/kg and 20 mg/kg. The mice were then irradiated with a fiber-coupled diode laser at 793 nm. 10 mg/kg of QDs gave 6.2℃ temperature rise whilst 20 mg/kg of QDs raised the surface temperature by almost 9 ℃ at 1.49 $W/cm^2$ of laser intensity. When the laser intensity was increased to 1.59 $W/cm^2$ and applied for 10 minutes, the temperature rise was recorded as 15℃. The experimental methods described in this thesis work should be useful in the characterization of new potentially important nanoparticles for photothermal therapy applications.

# ÖZETÇE


**Fotosensitizörlerin Fototermal Terapi İçin Dalgaboyuna Bağlı Fototermal Dönüşüm Verimliliği**

**Minahil Khan**

**Malzeme Bilimleri ve Mühendisliği Programı, Yüksek Lisans**

**24 Ocak 2021**

Kanser tedavisi, kanserin Dünya çapındaki en ölümcül ikinci hastalık olmasından dolayı, en önemli bilimsel araştırma alanları arasında yer almaktadır. Gelecekteki kanser tedavileri için güçlü potansiyele sahip birçok tedaviden bir tanesi, kanser hücrelerinin ısınma sonucunda yok edilmesini sağlayan fototermal terapidir (PTT). Işık ile uyarılan nanoparçacıklar, hem ısınma etkisi oluşturabildiklerinden, hem de belirli kanser dokularını hedef alarak kemoterapi ilaçlarını bu dokulara taşıyabildiklerinden, (PTT) için popüler fotosensitizörler haline gelmiştir. Nanoparçacıkların fototermal dönüşüm verimliliği, PTT'de terapötik kullanımlarının değerlendirilmesinde kritik öneme sahiptir. Bu tez çalışmasında, çözelti içerisindeki nanoparçacıkların fototermal dönüşüm verimliliğinin belirlenmesini sağlayan bir kolorimetrik yöntem geliştirilmiştir. Gümüş sülfür-glutatyon kuantum noktaları ($Ag_2S$-GSH QD'ler) içeren bir çözelti küvet içerisine konmuş, odaklanmış sürekli dalga lazer hüzmesi ile uyarılmış ve elde edilen en yüksek sıcaklık artışı kızılaltı kamera ile ölçülmüştür. Verilerin analizi için kendine özgü (intrinsic) ve dış (external) verim olmak üzere iki ayrı dönüşüm verimi tanımlanmış ve nanoparçacıkların oluşturduğu ısıtma gücü, sırasıyla soğurulan ve gelen optik güç ile ilişkilendirilmiştir. Dalgaboyu ayarlanabilen $Ti^{3+}$:safir lazeri ile yapılan ölçümler, $Ag_2S$GSH QD'lerin kendine özgü fototermal dönüşüm verimliliğinin 720−810 nm dalga boyu aralığında %91'i aştığını göstermiştir. Bu tez çalışmasında geliştirilen yöntem, ayrıca poli akrilik asit (PAA) kaplı süperparamanyetik demir oksit nanoparçacıklarının (PAA/SPION'lar) analizinde kullanılmış ve kendine özgü fototermal dönüşüm verimi 810 nm'de %83.4 olarak belirlenmiştir. 640nm'de, 600 µg/ml demir içeren PAA/SPION'ların, sırasıyla %76 ve %63'lük kendine özgü ve dışsal fototermal dönüşüm verimliliğine sahip olduğu görülmüştür. Bu tez çalışmasında geliştirilen deneysel yöntem, fototermal terapi uygulamaları için elverişli nanoparçacıkların değerlendirilmesinde kullanılabilecektir. Ek olarak yapılan in vitro deneylerde, $Ag_2S$-GSH Herceptin QD'ler, tümör (SKBR3) ile

büyütülen farelere enjekte edilmiştir. Cisplatin, QD'ler ile kemoterapötik ilaç olarak kullanılmıştır. Hem Cisplatin hem de $Ag_2S$-GSH Herceptin QD'ler fareye deri altından enjekte edilmiş ve farklı derişimlerin (10 mg/kg ve 20 mg/kg) etkisi incelenmiştir. Fareler daha sonra 793 nm'de fiber aktarmalı diyot lazeri ile uyarılmıştır. 10 mg/kg derişimde QD'ler 6.2°C sıcaklık artışı sağlarken, 20 mg/kg derişimde QD'ler, 1.49 W/cm$^2$ lazer ışınım şiddeti kullanıldığında, yaklaşık 9°C'lik bir sıcaklık artışı sağlamıştır. Lazer gücü değiştirilerek, sıcaklık artışının lazer şiddetine olan bağımlılığı da araştırılmıştır. Buna göre, 20 mg/kg derişimde $Ag_2S$-GSH Herceptin QD enjekte edilen farede, lazer ışınım şiddeti 1.59 W/cm$^{2'}$ye çıkarılıp 10 dakika süreyle uygulandığında, 15°C'lik sıcaklık artışı gözlenmiştir. Özetle, sunulan tez çalışmasında, $Ag_2S$-GSH Herceptin QD'lerin deri altına enjekte edilen tümör taşıyan farelerde oluşturduğu sıcaklık artışı incelenmiş, nanparçacıkların fototermal dönüşüm verimliliğini belirlemek için yeni bir sistematik yöntem geliştirilmiştir.

# AKNOWLEDGEMENTS

Firstly, I would like to extend my heartfelt gratitude to my kind, patient, and extremely supportive advisor, Prof. Dr. Alphan Sennaroğlu. His endless compassion, vast knowledge, and friendly guidance eased my path in studies as well as in accomplishing this thesis work. I would forever be in debt of him for the exposure he gave me to science and to a new culture. Especially, during the difficult times of pandemic, I was lucky to have constant meetings and discussions with him that kept me motivated and sane. I want to thank him once again for giving me a chance to live my dream and be a part of his Laser Research Group that became more like a family to me.

I would like to thank Prof. Funda Acar Yağcı, for giving me an opportunity to work and learn the applications of lasers. I would thank all her group members, whom I came to know during the collaborated work. It was a wonderful experience.

I am thankful to the group members of Laser Research Laboratory: Işınsu Baylam, Eylul Nihan Kamun, Ayşenur Torun, Suat Acli, and Faik Derya Ince, for their love, friendship, support, and knowledgeable discussions. A special thanks to my most favorite persons Yağiz Morova and Abdullah Muti who became my teacher, friend and guide during my Masters.

I am extremely grateful to my great and loving friend Nitasha Habib for giving me the best memories. I cannot thank her enough for being there in my difficult times and making quarantine time easier. I would also thank my other closest friend, Fatima Afra Muhammad Akram for all the help, joyful days, intellectual conversations and so many travel memories.

I would thank all my good friends Muhammad Panahi, Baseerat Roman Khan, Mariam Huda, Farhan Ali, Kamran Ullah for feeding me with their amazing cuisines and introducing me to their cultures. Also, I would thank Fatima, Hassan, Aleema, Anaya, Haisum, Hanna, Anam Rahim, Reenam Rahim, Areej, Mishal, Kashmine, Ishmal, Noor-ul-ain, and Faseeh Janjua for all the virtual support from miles apart.

I have no words to express my gratitude to my parents, especially to my mother who educated and supported me despite all the hardships. I could never return this favor, but I can always honor her struggles with my small tokens of success. I would thank my beloved sisters Aliyya Albab Khan and Ishmam Zarnab Khan for being so strong and becoming rocky support. Lastly, I would like to thank my Dada and Dado (grandparents) for keeping a check on me and making sure that I am living my best. I am blessed to have them in my life.

# TABLE OF CONTENTS

# LIST OF FIGURES

# ABBREVIATIONS

| | |
|---|---|
| PTT | Photothermal Therapy |
| PDT | Photodynamic Therapy |
| QD | Quantum Dots |
| PS | Photosensitizers |
| NIR | Near infra-red |
| IR | Infra-red |

# CHAPTER 1:
# INTRODUCTION

## *1.1 Application of Lasers in Medical Treatments*

In the field of medicine, two stages are important for the betterment of human health: one is diagnosis at the earliest stage possible and the other is treatment of the disease with selective targeting of diseased area without causing any damage to healthy tissues. Light can be used quite well for both purposes. In early ages, light sources (sun, fire) were used in the treatment of many diseases. In 1400 B.C, Hindus used to layer herbs over the human body and expose it to sunlight. Multitude of diseases were treated with heliotherapy by ancient physicians of Egypt, Rome, and Greece [1]. However, discovery of lasers in the last century has completely revolutionized the diagnosis and the treatment methodologies. It has given a huge margin to control, manipulate, and play with the properties of light. In the diagnosis applications, lasers can be used as an optical imaging tool for tomography such as optical coherence tomography, diffuse optical tomography and optical spectroscopy. For the purpose of treatment, i.e., surgery and therapy, laser can be used in the treatment of various diseases such as renal surgery, eye surgery, acne treatments and liver stones [2]. Initially, the laser was first used in 1961 to treat skin melanoma [3][4]. Then, in 1965, $CO_2$ laser was invented and extensively investigated for cutting applications. Later, Polanyi used $CO_2$ laser for cutting the polyps on vocal cords in 1968 which opened the wide horizons of lasers in medicine and surgery [5][6]. During the same year, Nath successfully coupled a laser source to the optical fiber that introduced lasers in the realm of diagnosis such as endoscopy. In 1981, lasers were used clinically and pre-clinically in the treatment of cancers through ablation of tumors such as brain, pancreas, liver and prostrate tumors [8, 9]. The working principle of these surgical and therapeutic applications involves absorption of laser light, resulting in energy deposition in cells [10, 11]. Some other prominent types of lasers currently used for surgery are Nd:YAG and Argon lasers. Similar to $CO_2$ laser, Nd:YAG is also suitable for ablation of tumor tissues. Argon laser is used for the treatment of eye tumors and to block wounds or blood vessels to stop bleeding.

In therapeutic application of lasers, there are three different therapeutic ways, known as photothermal therapy, photomechanical therapy, and photochemical therapy. In these methods, energy deposition from laser light helps in killing cells. Specifically, in the photothermal therapy, laser absorption kills the abnormal cells by increasing their temperature. Examples include hyperthermia for cancer treatment and coagulation of blood vessels. In the photomechanical effect, shock or mechanical waves are produced after absorbing laser light. The good examples of this therapeutic method are renal surgery and tissue removal through vaporization. Then in photochemical effect, the laser light is absorbed to produce electronic excitation of chromophores. Photodynamic therapy and light activated dental filling are the common examples of the therapeutic applications [12].

In the medical applications discussed above, it is also important to specify the type of the laser used and its operating parameters. The laser has many parameters that are crucial for applications in medicine. The following set of parameters should be specified precisely for the repeatability of the medical procedure:

**1)** The type of laser used (for example, solid-state laser or diode laser).

**2)** Regime of operation (for example, continuous-wave operation or pulsed operation).

**3)** The spectral range and wavelength of choice: there are certain spectral ranges known as biological windows in which absorption and scattering are comparatively low and light transmission in the tissues improves. For example, skin and hemoglobin have lowest absorbance between 650-900 nm and maximum transmission is around 800 nm [13]. Based on the types of medical applications, biological windows are categorized as I, II, III and IV-windows. The most conventional one is the near infrared (NIR) window-I (NIR-I window) that ranges from 750-1000 nm. In this range, the laser-tissue interaction is considered as the safest for the living cells due to its non-ionizing nature. The second optical window-II (1000-1400 nm, also known as the NIR-II window) has also been widely investigated due to its deeper penetration in tissues [14]. The third optical window (1600-1870 nm) as well as the fourth optical window (2100-2300 nm) that has high water absorption has also been used for biological applications. The

fourth window has its applications in treatment of osteoporosis and vulnerable plaque and skin cancer [15]. Lasers operating in the NIR I and NIR II regions have extensive medical applications such as (a) control of gene expression in cells [16], (b) optically guided liquid flow in microfluid pathways [17], (c) monitoring of drug delivery systems [18], (d) eradication of tumor cells by various thermal effects such as ablation, necrosis, coagulation and desiccation [19].

**4)** Power of the laser: if the laser being used is continuous-wave, then its output power is measured in watts. In the case of pulsed lasers, the average power, pulse duration and repetition rate are important.

**5)** How the laser beam is being applied to the target: there are two categories of beam application. One is contact and the other is non-contact irradiation. Contact irradiation requires information of pressure applied and non-contact irradiation requires knowledge of the distance of laser source from the target.

**6)** Spot size of the laser beam for in-vitro and irradiated area is significant for in-vivo experiments because the light intensity on the tissue will vary with spot-size if the power is constant.

**7)** Time or duration of irradiation should be known.

All the above-mentioned parameters are important during laser therapy. On the basis of these parameters, intensity, energy density or power density can be calculated [20]. Furthermore, Figure 1.1 shows some additional factors, such as optical properties (absorption, scattering, refractive index) and physical properties (geometry) of the cell, all of which play a crucial role in laser-tissue interaction and hence, in medical applications.

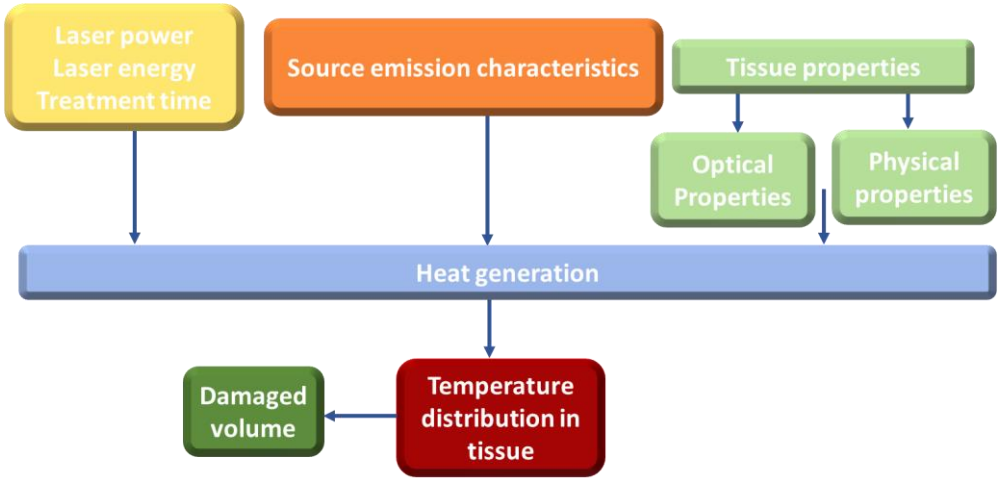


Figure 1.1 Factors influencing the laser tissue interaction

In this thesis, we discuss the application of lasers for the treatment of cancer based on photothermal therapy (PTT). Cancer is abnormal growth of cells accompanied by deactivation of the genes that fight against cancer [21]. There are two factors that play important role in cancer treatment, one is the early diagnosis and the second one is the survival rate of the cancer type. Most of the deaths are caused due to late diagnosis of cancer. In 2020, lung cancer caused 1.80 million deaths, colorectal cancer killed around one million and liver cancer took 0.8 million lives worldwide. If diagnosed on time, lung, colorectal and liver cancer are treatable cancers with good survival rates [22] whereas, the most dangerous cancers with low survival rates are skin cancer, breast cancer, and prostate cancer. According to the US statistics reported in 2018, improvement in early diagnosis of cancer and its advanced treatment methodologies have reduced the death rate by 31% in 21$^{st}$ century as compared to 20$^{th}$ century, when cancer cases peaked in 1991 [23]. To combat cancer mortality, various treatment methods have been adapted so far.

One of the oldest treatments for cancer is surgery that is still being used to cure many cancers. This methodology helps to remove any solid tumor present in any organ of the body. Further, colectomy for bowel cancer, craniotomy for brain cancer, cystectomy for bladder and gastrectomy for stomach cancer are some of the surgical procedures that can be performed to treat cancer. Success of excisional surgeries also depends on the advancement of cutting tools and corresponding techniques [24]. The other treatment is chemotherapy in which strong drugs are used to kill the cancer cells, but it is not a tumor

specific therapy. Therefore, it damages the healthy cells and causes severe side effects. These chemo drugs can also be used in small amounts after surgery to kill the remaining cancer cells. In this way, side effects due to excessive usage of chemo-drugs can be minimized. Third method of treating cancer is radiotherapy which kills or shrinks the cancer cells by exposing them to radiation. Intense ionizing radiation damages the DNA of cells beyond repair, leading them to death. Radiotherapy does not cause immediate death of cancer cells; it takes multiple irradiation sessions to completely remove them. There are two kinds of radiotherapies: internal radiotherapy and external radiotherapy. In internal radiotherapy, the radiation source is placed inside the body while in external radiotherapy the source is adjusted outside the body which revolves around the body to target cancer cells. Like surgery, radiotherapy is also beneficial for treating localized tumors. Surgery, chemotherapy and radiotherapy are conventional methods of treating cancer. However, these methods have fair disadvantages as well. These methodologies damage healthy cells and reduce immunity, as a result of which probability of having another cancer increases. Hence, quest for a better treatment modality never seized in the field of cancer treatments, which lead to the emergence of two methods known as photodynamic therapy (PDT) and photothermal therapy (PTT). Both are localized therapies, non-invasive and more effective when used in combination with chemotherapy and radiotherapy.

## *1.2 Photodynamic Therapy (PDT)*

Photodynamic Therapy (PDT) is the cell death mechanism in which singlet oxygen generation reduces the number of living cells. In PDT, as only single oxygen molecule is excited, it needs comparatively low amount of energy.

Photodynamic therapy has its major application in cancer treatment, due to its non-invasiveness, minimum side effects, low toxicity and higher selectivity [25]. This therapeutic effect occurs by filling up the tumor with photosensitizer (PS) and then irradiating the tumor at a suitable wavelength in the biological window. The light activates the PS in the presence of reactive oxygen species (ROS) that would ultimately cause phototoxicity [26, 27] as shown in figure 1.2. The ROS reacts with the organelles such as mitochondria, vacuole and centriole to initiate cell death mechanisms (necrosis and apoptosis).

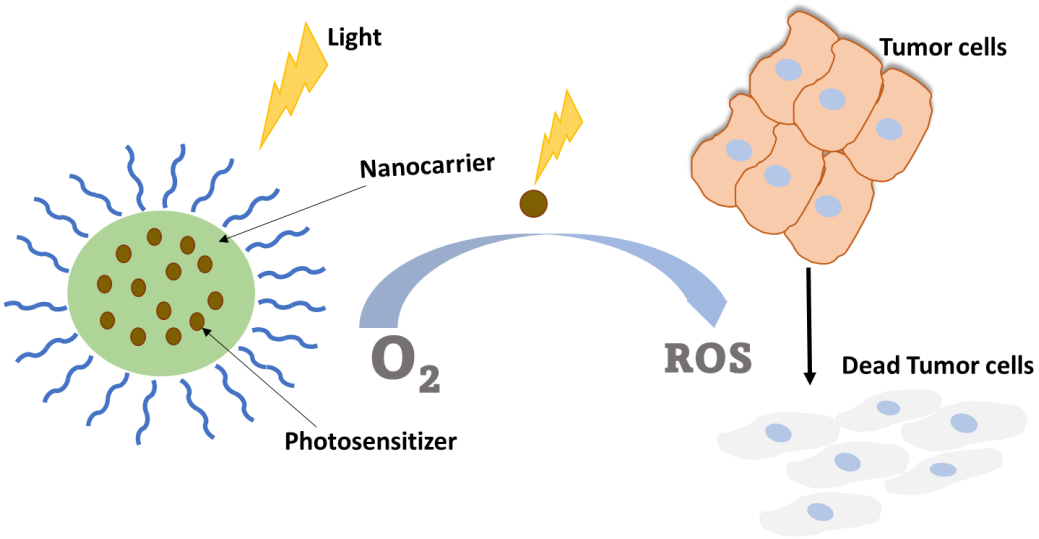


Figure 1.2 A schematic of the procedure of tumor death via photodynamic therapy

PDT becomes highly effective if the light penetrates enough into the tumor cell and adequate PS is injected into the tumor area [28]. Light penetration into a cell results in many phenomena such as reflection, absorption, transmission and refraction [29]. As it is hard to change the optical properties of cells, it is important to choose the suitable wavelength of light with high absorption for PDT, which further depends on the choice of PS and its absorption capabilities [30]. Absorption of photosensitizers should be high enough to form singlet oxygen. To activate photosensitizers, many irradiation sources can be used such as light emitting diode (LED), lamps and lasers. Lasers have more advantages over the other sources because they are monochromatic and have high brightness [26, 28].

In 1904, Von Tappeiner and Jodblauer began to explain the oxygen-consuming chemical fluorescence after injecting aniline dyes in protozoa, and coined the term "photodynamic effect"[31, 32]. The very next year, Von Tappeiner and Jesionek used 5% eosin as a topically administered PS to treat skin cancer [31, 33]. Figge and colleagues discovered that hematoporphyrin was particularly concentrated in cancerous, embryos, and psychologically damaged tissues, and it quickly became a standard photosensitizer (PS) for PDT [31]. In 1978, red light was utilized for photoactivation to treat skin cancer [33]. Photodynamic therapy with different light sources is not something recently discovered, ever since, photodynamic therapy has been used for treatment of coronary and contagious disease as well as osteo-arthritis, bowel and cornea cancers [33-35].

For effective photodynamic therapy, choice of photosensitizer (PS) that has high water solubility, good biodegradability, no toxicity and has no impurity is important. Since PS are expected to circulate in blood and accumulate sufficiently in the tumor site, they must have suitable properties such as good circulation time and rapid degradation [26, 36]. Photosensitizers have three generations, the first one consists of the nanoparticles that have absorption at ~400 nm. Such nanoparticles do not have absorption in the infra-red (IR) region, so light cannot penetrate much into the tissues [26, 36]. Therefore, second generation of photosensitizers is introduced that has absorption in visible (above 600 nm) and NIR region of the light. This generation has very good absorption in red region (IR), however, it has very low tumor specificity [26]. Hence, third generation of photosensitizers came into being that had potential to circulate fast and have high accumulation in the tumor region [36, 37].

## *1.3 Photothermal Therapy (PTT)*

Photothermal therapy (PTT) is a therapeutic method that causes the death of tumor cells like PDT; however, it increases the temperature of the cell leading to its death. When photosensitizers are injected into the tumor cell, they absorb light irradiated on the tumor site. Ultimately it results in photocoagulation or cell death by temperature increase as shown in the figure 1.3.

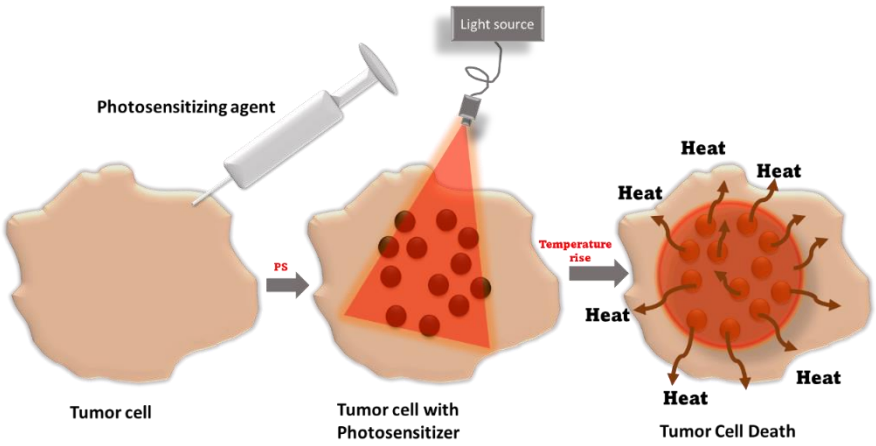


Figure 1.3 Tumor cell death mechanism by photothermal therapy.

Cell death by thermal therapy can be done in three ways based on the increase in temperature and the duration in which that temperature is maintained. The first way is called diathermia in which temperature of the cell is raised by high-frequency electric

current which causes blood clotting to destroy the unhealthy cell. Second way is hyperthermia in which temperature of a cell is increased so much that thermoregulation of cell fails to handle it and collapse the cell structure. Hyperthermia can be caused by any heating source if it can raise its temperature nearly up to 48 ℃. Third way is thermal ablation, which is extreme hyperthermia. All these methods of thermal therapy have one hindrance, that is to confine temperature increase within the cell [38].

In recent years, photothermal therapy (PTT) has received a great deal of attention due to its promising potential as an alternative and versatile local treatment modality for cancer [30, 39-42]. Tumors have less heat tolerance as compared to normal tissues, so PTT is very effective in killing them. However, light sometimes can change enzyme reactions that results in catalysis, therefore, it is important to choose light wavelength and intensity carefully to avoid any damage to healthy tissues [29, 43, 44]. PTT involves irradiation of tissue containing a photosensitizer (PS) with a near-infrared (NIR) laser, typically operating around 800 nm, causing an increase in the local temperature beyond a threshold level, where various mechanisms such as protein denaturation and/or cell-wall damage can lead to the death of cancer cells [45-47]. Several favorable aspects of PTT include (1) potentially low risk of damage to healthy tissue due to the nonionizing nature of the NIR laser source, (2) higher penetration of the NIR light into the tissue, in comparison with visible or ultraviolet light due to reduced scattering, (3) spatial selectivity of the method, whereby tissue heating occurs only in those regions where the otherwise inactive photosensitizer is irradiated, (4) no collective toxicity, and (5) stimulation of the immune responses [25, 30]

### *1.3.1 Photothermal Therapeutic (PTT) Agents*

Recent research has focused on the development of new biocompatible PSs activatable in the NIR that enable efficient heating of the tissue for cancer treatment and eradication of highly resistant bacterial types [48, 49]. Nanoparticles are very promising candidates as PTT agents. Recently studied nanoparticles for PTT include plasmonic gold and silver nanoparticles [50-52], carbon nanotubes, graphene family nanomaterials, and fullerene-silica nanoparticles [53-55], to name a few. Superparamagnetic iron oxide nanoparticles

(SPIONs) have also become highly popular since they are trackable by magnetic resonance imaging and are active under NIR irradiation [56, 57]. Similarly, $Ag_2S$ quantum dots (QDs) with luminescence in the NIR and PTT activity at NIR wavelengths are popular as well [56, 58]. These $Ag_2S$ QDs can provide optical-image-guided PTT, which is advantageous in clinical studies. Hence, nanoparticles that can induce PTT, such as $Ag_2S$ QDs and SPIONs, with the added benefit of tumor targeting via enhanced permeability and retention (EPR) effect and large surface-to-volume ratio, allowing conjugation of tumor-specific ligands and even drugs, are in the spotlight for PTT and combined PTT/ chemotherapy applications.

## *1.4 Importance of Photothermal (PTT) Efficiency*

Accurate measurement of the photothermal conversion efficiency plays a central role in the assessment of NPs as PS's for PTT. This is because, despite the nonionizing nature of the NIR laser used in PTT, thermal damage risk of healthy tissues still exists, especially if excessive power levels are needed to achieve the desired temperature rise. Ideally, the photosensitizer should have a high photothermal conversion efficiency to minimize the required incident power for the tissue. In addition, it is also highly desirable to develop PS's with large absorption cross sections so that low concentrations of the PS's within safe limits and low laser power levels are sufficient to achieve the desired temperature rise. These stringent requirements call for the development and use of systematic measurement protocols to determine the photothermal conversion efficiency of the PSs. To date, numerous techniques have been utilized to determine the photothermal conversion efficiency and have been applied to the characterization of different PSs [50, 59].

Since we used glutathione-coated $Ag_2S$ QDs ($Ag_2S$-GSH) to calculate photothermal conversion, we note that experimentally determined photothermal conversion efficiencies reported in the literature vary over a significant range. Based on the most widely used model reported by Roper et al. [60], the photothermal conversion efficiency of these QDs was determined to be 80%. Previously, Gao et al. showed in vitro and in vivo PTT and optical imaging applications of water-soluble Aptamer 43 tagged $Ag_2S$ QDs and reported a photothermal conversion efficiency of 23.8% [61]. In another study conducted by Zhao

et al., $Ag_2S$ QD-polypeptide hybrid nanogel ($Ag_2S$ QD@PC10ARGD) exhibited 28.7% photo thermal conversion efficiency under 810 nm laser irradiation [62].

## *1.5 Description of The Measurement Method of Photothermal Conversion Efficiency*

In this thesis work, an accurate, systematic method for the determination of the photothermal conversion efficiency of NPs in solution is described and applied to the analysis of silver sulfide-glutathione QDs ($Ag_2S$-GSH QD). In the experiments, a cuvette containing a solution of $Ag_2S$-GSH QD was irradiated with a tightly focused laser beam, and the resulting temperature rise was determined by averaging the steady-state temperature distribution on the cuvette surface, recorded with an infrared camera. The incident power of the laser and the cuvette/solution mass were adjusted to limit the maximum temperature rise to below 15 °C so that a linearized heat transfer model could be used to analyze the heating data. Our analysis method is a modified version of that reported by Roper et al and provides efficiency expressions in terms of the total laser beam power. The use of a tightly focused laser beam inside the cuvette thus eliminates the need to know the exact spatial distribution of the irradiation intensity. Two different photothermal conversion efficiencies, $\eta_i$ and $\eta_{ext}$, were introduced to relate the induced heating power of the nanoparticles with the absorbed and incident light power, respectively.

## *1.6 Overview of The In vivo Experiments*

After successful calculation of photothermal conversion efficiency of $Ag_2S$ QDs in solution, the next phase was to investigate intertumoral NIR absorption. In past, the trials on different cell lines and prediction of its potential for clinical application started in early 1970s [63]. The aim was to achieve mild local hyperthermia, the condition in which temperature of the cell reaches up to 41-42 ℃ [64]. It has been found that photothermal therapy gives its best results in combination with other therapies such as chemotherapy and radiotherapy.

In photothermal therapy, to attain the localized temperature rise for killing tumor cells, without any damage to healthy tissues, a suitable combination of therapeutic drug dose, photothermal agent (with reasonable photothermal conversion efficiency) and laser intensity is required [13]. Several therapeutic drugs have been discovered so far but a few of them are alkylating agents, platinum compounds, doxorubicin, fluorouracil, taxanes, vinca alkaloids and cisplatin [64]. However, to increase the body temperature from 37 ℃ to 41 ℃ (hyperthermia), different factors must be considered such as mass to body ratio, core body temperature and intensity of light used for irradiation; therefore, this subject is still under study and no profound standards have been decided yet [65]. Generally, temperature of the living body depends on the metabolism. If the body temperature is increased its metabolism will decrease to produce less heat and to maintain the temperature. Similarly, if the temperature is reduced, metabolism (breathing rate, heart rate) will increase. When a body is at complete rest, it still consumes energy that is called basal metabolic rate also known as BMR (the minimum amount of energy that a living body needs from environment for its survival), it is also worth noting that BMR increases in mammals as body mass decreases [66]. In the living body, the temperature increase for clinical procedure is decided by the method called SAR (W/kg), known as power density specific absorption rate [67]. SAR also depends on characteristics (type, frequency) of radiations and BMR value. For human body, average BMR value is above 1 W/kg while it is 10 W/kg for a mouse [66] .Mathew G skinner *et al.* gave formulas to calculate SAR for different sources (laser, microwave, ultrasound) [68]. Another factor that affects hyperthermia is called perfusion. Perfusion (to bathe tissue, cell or organ with anticancer fluid) resists the increase in temperature. The general perfusion rate of human tumor cell is around 5-15 ml per 100 gram per minute, however, it differs greatly for different tumor cells. So, power density required to obtain mild hyperthermia (<~42$^{o}$C) is 20-40 W/Kg [64].

For the in-vivo experiments, the choice of animal is significant that means it should have close resemblance to the human genome [69]. In that perspective, mouse is an extremely important specie for the scientific research as has quite similar genes as human beings i.e., it is a mammal and an endotherm. In past two decades, there is a drastic increase in reported studies that utilized mouse as a medium to predict the implementation of the obtained experimental data on humans [66]. Besides the genome, the metabolism of

mouse shares so many similar characteristics with human body, that are not found in other species [70]. Considering that, in photothermal therapy the temperature increase of the tumor is monitored which is implanted in the mouse, so body temperature of the mouse becomes point of attention because it affects metabolism, heart rate and drug efficacy and other various functions. Although, mouse is considered to have stabilized thermoregulation, yet its thermal physiology poses challenges for researchers due to 1) fluctuations in core temperature 2) high metabolism 3) preferring ambient temperature to be warm 4) high thermal conductivity 5) huge difference in the body to mass ratio 6) large surface area. All these factors play a vital role in the measurement of temperature and its interpretation for the human body. Figure 1.4 shows the chart of similarities and differences. Although, the difference between average temperature of human being and a mouse is around 1 °C, but repeated temperature sampling of mouse under standard laboratory and housing conditions depicts that core temperature fluctuates between 3-4 °C within 30 minutes. This change in temperature can be reduced by increasing the ambient temperature, however, fluctuation will persist at thermoneutral zone as well as at laboratory standard temperature conditions [71].

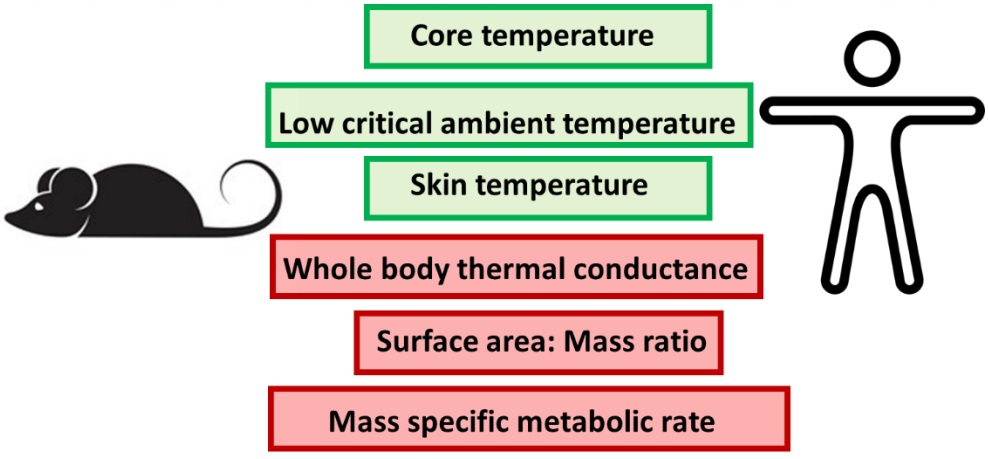


Figure 1.4 A chart of similarities and differences vital for thermoregulation in the *in vivo* experiments with mouse. Red shows differences and green shows similarities.

From this discussion it should not be inferred that highly fluctuating thermoregulatory system of mouse makes it unsuitable for *in vivo* experiments. Instead, it stresses on the point that all stimuli that affect thermoregulation must be considered in thermal therapies especially when ambient temperature fluctuates. In short, the regulation of core

temperature is not fixed but highly dependent on environmental factors [72]. For photothermal therapy, after the stabilization of thermoregulatory system of the tumor bearing mouse, procedure of laser irradiation is considered.

In general, laser irradiation of mouse and other living beings depend on four parameters. Wavelength of light, intensity of light, beam cross-section area, and total time of irradiation [73]. For localized mild hyperthermia, the most suitable wavelength range is NIR I, the cross-section area of the beam is kept in such a way that it only irradiates the tumor area. The safe power density according to American National is reported as ~0.7 W/cm$^2$ for 980 nm and 0.33 W/cm$^2$ for 808 nm [30]. However, in literature the intensities have been used within the range of 0.5-2 W/cm$^2$ [74-77].

The method described in this thesis is not suitable for the in vivo measurement of photothermal conversion efficiency. This is because in the case of in vivo measurements, the irradiated region is not isolated, making it difficult to determine the effective mass of the tissue containing QDs. Furthermore, more sophisticated computational methods are necessary to model the heat transfer processes and to calculate the amount of light scattering from the tissue surface as well as overall attenuation within the tissue.

## *1.7 Summary:*

Basic light sources, such as sun and fire have been utilized in treating different diseases for ages. After the invention of lasers, the applications of light in medicine have been completely revolutionized. Nowadays, lasers are used in diagnosis, imaging, surgery as well as non-invasive therapies. Two important therapies, namely, photodynamic and photothermal therapies utilize laser to treat cancer affected patients, the deadliest disease around the globe. In 2020, 19.3 million cancer cases were reported and 10 million patients could not survive [78]. So far, the clinically accepted cancer treatments are surgery, chemotherapy and radiotherapy but they have side effects such as destruction of normal cells and weakening of immune system. These treatments may also increase the chances of another cancer [79-81]. Therefore, photodynamic and photothermal therapy have formed a hot research topic for the past few decades as they have synergistic effects, and provide localized treatment of the tumor without damaging the healthy tissues. In

photodynamic therapy singlet oxygen is produced by the irradiation of light which destroys the cell whilst in photothermal therapy, temperature of the tumor is increased to cause cell death. There are many photosensitizers for this therapeutic method and the particular one studied in this thesis is $Ag_2S$-GSH. This nanoparticle has good biocompatibility and no toxicity. Careful characterization of the photothermal nature of the nanoparticle and the measurement of photothermal conversion efficiency play a crucial role in the development of these nanoparticles for practical medical treatment applications.

# CHAPTER 2:
# EXPERIMENTAL SET UP

## *2.1 In vitro Experiments*

The experimental set up for the measurement of photothermal conversion efficiency is shown in Figure 2.1. A homemade, continuous-wave, $Ti^{3+}$:sapphire laser was used to generate tunable coherent radiation in the 720−810 nm wavelength range. The x-shaped resonator consisted of a 20 mm long, Brewster-cut $Ti^{3+}$-doped sapphire crystal, which had an absorption of 92% at 532 nm, located between two curved mirrors (C1 and C2, each with a radius of curvature of 100 mm). The resonator was completed with a flat high reflector (HR) and a 15% transmitting output coupler (OC). A pair of Brewster-cut dispersive SF10 prisms (P1 and P2) were inserted in the HR arm to vary the output wavelength of the laser. The $Ti^{3+}$:sapphire laser was end-pumped with a 5 W, 532 nm green pump laser, whose beam was focused with an input lens (L1, with focal length f = 100 mm) into the $Ti^{3+}$:sapphire crystal and generated up to 1 W of continuous wave output power at 778 nm. A series of highly reflecting flat mirrors (M3−M4), a concave high reflector (M5, radius of curvature = 200 cm), and a converging lens (L2, f = 200 mm) were then used to direct the output of the $Ti^{3+}$:sapphire laser into the cuvette (C) containing the nanoparticle solutions. The power of the $Ti^{3+}$:sapphire laser could be varied continuously using a half-wave plate (HWP) and a polarizing beam splitter (PBS).

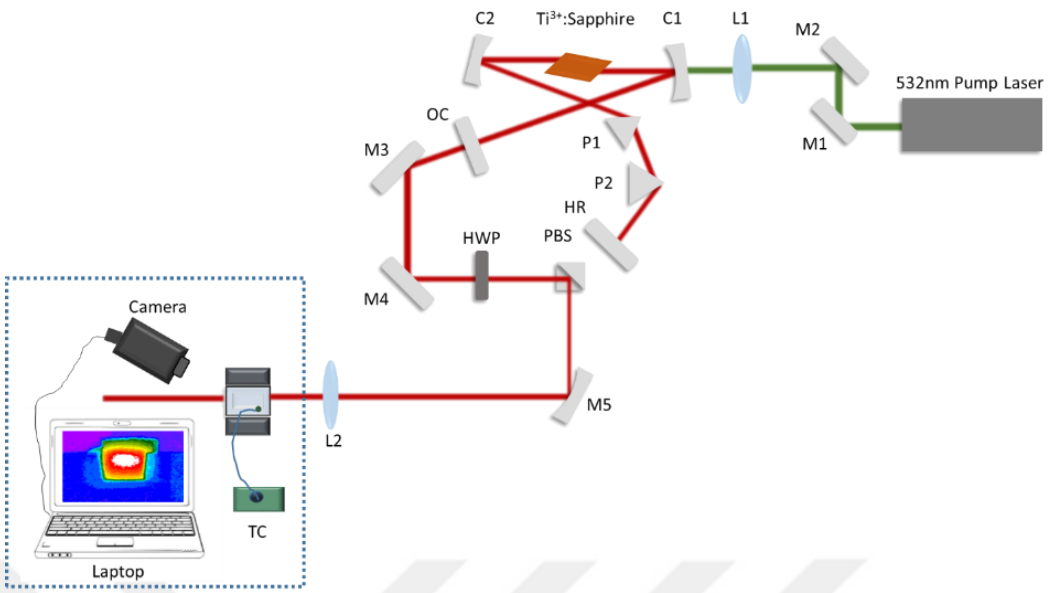


Figure 2.1 Schematic of the experimental setup used in the wavelength-dependent photothermal conversion efficiency measurements.

A more detailed sketch of the photothermal conversion efficiency measurement setup is further shown in Figure 2.2. The incident laser beam was focused with a converging lens (L2 in Figure 2.2, focal length f = 200 mm) to a beam waist ($w_0$) of 25 μm at the distance of about 5 cm after the cuvette. The polished input ($w_i$) and exit ($w_e$) windows of the polystyrene cuvette allowed the passage of the laser beam, whereas the sides and the bottom of the cuvette were surrounded with a 4 mm thick rubber insulation to minimize heat loss. The unfilled portion of each cuvette was cut so that the overall volume of the cuvette was only about 6% more than the volume of the solution used in the experiments to minimize the conductive heat transfer into the unfilled section of the cuvette. A thermocouple (TC) probe was dipped into the solution to record the variation of the solution temperature as a function of time. Care was taken so as not to overlap the thermocouple with the propagating laser beam in the solution.

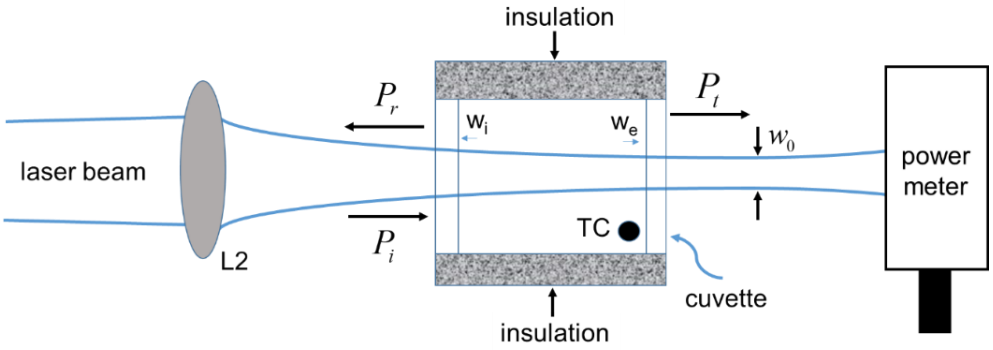


Figure 2.2 Details of the photothermal conversion efficiency measurement setup. See the text for a description of the abbreviations.

The procedure detailed below was followed for the heating experiments:

(1) At each chosen output wavelength $\lambda_L$ of the laser, the incident ($P_i$), reflected ($P_r$), and transmitted ($P_t$) powers were measured. The half-wave plate (HWP) was rotated to adjust the incident power (Pi) so that the power $P_0$ coupled into the cuvette ($P_0 = P_i - P_r$) was about 200 mW for each measurement. The length of the cuvette was 10 mm.

(2) Because the thermocouple measures the temperature at a specific location within the solution, the time-dependent temperature data recorded with the thermocouple were used only to determine the time constant $\tau_h$ for heating. During the heating cycle, once the steady-state maximum temperature was reached based on the thermocouple reading, the maximum temperature rise of the solution was then determined using an infrared camera (FLIR, model no. A325SC).

(3) In the experiments, the wavelength of the $Ti^{3+}$:sapphire laser was varied in 10 nm steps between 720 and 810 nm, and the above-mentioned temperature measurement procedure for QD solutions was repeated at each wavelength.

(4) The temperature measurement was repeated three times at each wavelength. In each case, a new polystyrene cuvette was cut to the right size as explained above and filled with about 0.9 g of Ag2S-GSH QD solution with a fixed concentration of 5 mg/mL. Since the cuvettes were manually cut, the mass of each cuvette ($m_c$) was separately measured. The mass of the solution before and after each heating experiment was

further measured with an accurate balance (Sartorius, model AX224) and the average value was used as the solution mass ($m_s$) in the efficiency calculations.

(5) At each laser irradiation wavelength between 730 and 810 nm, the maximum temperature increase was further measured for the cuvette containing pure water.

To demonstrate the applicability of the method to the study of other nanoparticles, the photothermal conversion efficiency of poly(acrylic acid)-coated superparamagnetic iron oxide nano-particles (PAA/SPIONs) was also measured at 810 nm. In the experiments, six different cuvettes, each containing an aqueous solution of PAA/SPIONs at 39.4 mg/ mL Fe concentration were used. The average initial mass of the solutions was 0.89 g. The average power $P_0$ coupled into the cuvette ($P_0 = P_i - P_r$) was 204 mW. The power reflection (R) and transmission (T) of the solution were measured to be 5.1 and 6.5%, respectively. The same procedure as in the case of Ag2S-GSH QDs was followed and the measurement at 810 nm was repeated with six different samples to test the repeatability of the measurement protocol.

We built another setup to perform similar measurements with above mentioned steps at 640 nm. This set up consists of a 640 nm red fiber coupled diode laser. Two lenses L1 (with focal length f = 1.336 cm) was used to collimate the beam and L2 (focal length f =2.5 cm) was used to focus and couple the beam with the fiber. After coupling the laser beam, it was collimated and directed into the polystyrene cuvette by the lens (L3 with focal length = 2.5 cm) and a parabolic mirror (EFL=10.16 cm). The spot-size of the collimated laser beam was measured as 1680 μm in horizontal axis and 1280 μm in vertical axis by utilizing knife-edge method just before the cuvette. The schematic of set up is shown in Figure 2.3. This set up was used to measure the temperature change in polyacrylic acid coated super-paramagnetic iron oxide (PAA-$Fe_3O_4$ also known as PAA/SPIONS). Iron concentration in the solution was 600 μg/ml.

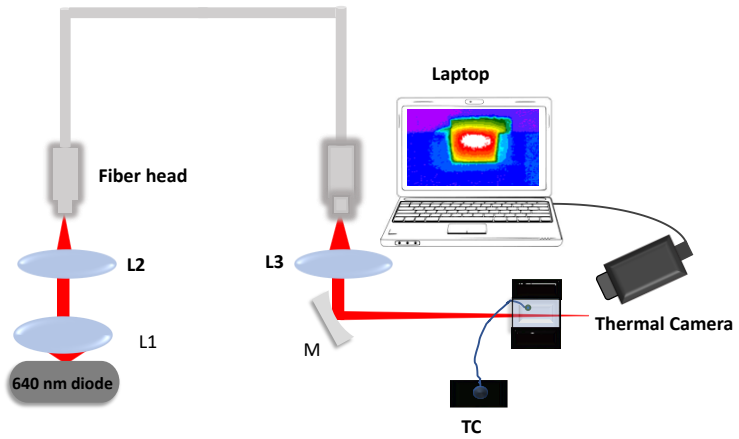


Figure 2.3 Schematic of experimental set up for photothermal conversion efficiency at 640 nm

## 2.2 *In vivo Experiments*

Over the course of time various optimizations were done to the experimental set up to reach the most suitable one that is explained here. For in vivo experiments a fiber coupled diode laser with the wavelength of 793 nm was used to irradiate tumor SKBR3 bearing mice for observing mild hyperthermia by using an FLIR camera. To keep the mice still during the irradiation, isoflurane (2-3%) was used as an anesthesia. Due to anesthesia, the temperature of the mice body was decreasing. Living body tends to lose heat due to low physical activity and slow metabolism under anesthesia [82]. So, the first step was to optimize the setup to maintain a higher ambient temperature (25℃) than the standard laboratory temperature (19 ℃ in our case). At first, commercially available apparatus such as heating pad (Physio Suite) was used but that was not suitable for temperature dependent experiments. Normally, heating pads are utilized in surgeries where the heat loss is huge due to direct exposure of internal organs to the environment along with anesthesia. In our case, the temperature was adjusted by two ways. 1) Controlling the ambient temperature by isolating the set-up from surrounding with a plexi-glass box and temperature of the box was maintained around ~25 ℃ by using a heating lamp. 2) Anesthesia (isoflurane) was given with a mask rather than injection as it is easy to get organism back to consciousness with the inhaled anesthesia. Due to slightly larger diameter of mask compared to the face of the mouse, some of the isoflurane was leaking

from the sides and causing further cooling in the surrounding. This problem was resolved by putting a surgical tape.

After optimization of the set-up to control temperature fluctuation, $Ag_2S$-GSH-Herceptin QDs were injected in multiple ways (subcutaneous, intertumoral, intravenously) into the mice and irradiated with 973 nm laser to see the magnitude of laser light absorption within living body conditions. In early experiments, the intensity used was 1.49 W/cm$^2$. For the subcutaneous studies of QDs and cisplatin, four tumor bearing mice were divided into two groups. First group had cisplatin with different QD doses in each mouse while second group was cisplatin free with similar doses as first group. In first group, one mouse had 10 mg/kg of $Ag_2S$-GSH-Herceptin QDs while second mouse had 20 mg/kg of $Ag_2S$-GSH-Herceptin QDs with cisplatin on the other hand mice in second group were also injected with 10 and 20 mg/kg $Ag_2S$-GSH-Herceptin QDs doses respectively but both were cisplatin free. After monitoring the effect of doses and Cisplatin, we increased the intensity from 1.48 W/cm$^2$ to 1.59 W/cm$^2$ to see change in temperature rise. Afterwards, experiments were repeated with intertumoral injections of QDs and cisplatin in three mice with a reduced dose of 30 mg/kg and two mice with only cisplatin (0.70 mg/kg) to make sure no significant heating is due to Cisplatin at 1.59 W/Cm$^2$ and all mice were kept under careful observation for 2 weeks to make sure that no damage was done by irradiation to the skin tissues. The schematic of the set-up used for this experiment is shown in Figure 2.4.

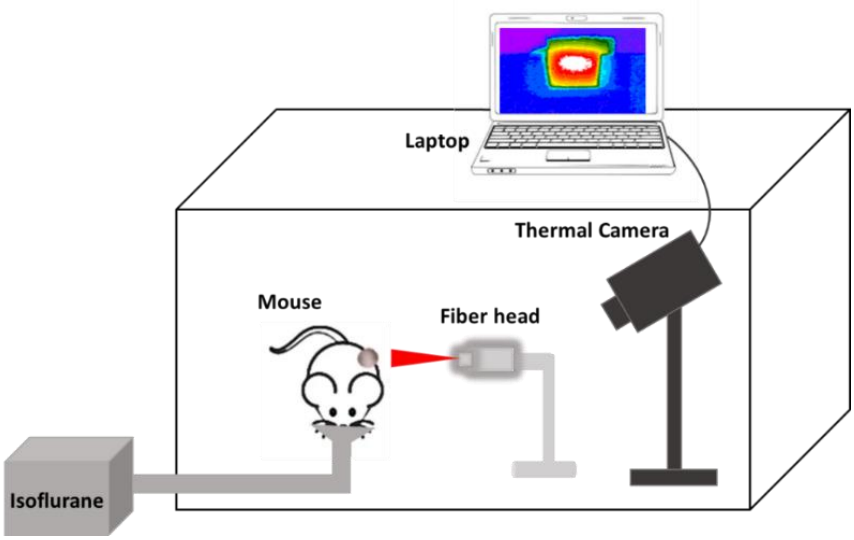


Figure 2.4 Sketch of experimental set up used for in vivo experiments performed on mice to see photothermal effect of $Ag_2S$-GSH-Herceptin QDs.

# CHAPTER 3:
# DERIVATION OF INTRINSIC AND EXTRINSIC PHOTOTHERMAL EFFICIENCIES

This chapter introduces two types of efficiency factors for the heating induced by nanoparticles during laser irradiation and describes a systematic analysis scheme that can be readily used by experimentalists without requiring sophisticated computational modelling of the heating process. As such, we assume that the system composed of the cuvette and the nanoparticle solution can be treated as a lumped element and solve a linearized heating model to determine the steady-state maximum temperature rise. To ensure consistency with the lumped model, an infrared camera was used in the experiments as described before to measure the average of the steady-state maximum temperature rise over the cuvette surface. This averaged maximum temperature rise was then used in the determination of the conversion efficiencies. We further assume that the laser beam propagating through the solution was well contained within the cuvette, so that the efficiency can be expressed in terms of the beam power.

Referring to Fig. 1(b), we assume that a Gaussian laser beam propagates through the solution with an intensity profile $I(r,z)$ given by [83]

$$I(r,z)=\frac{2P_0}{\pi w^2(z)}\exp\left(\frac{-2r^2}{w^2(z)}\right)\exp[-\alpha z]\ , \qquad (1)$$

where $r$ and $z$ designate the coordinates along the radial and propagation axes (see Fig. 1(b)), $P_0$ is the incident pump power on the right-hand side of the input window $w_i$ (at $z=0^+$), $\alpha$ is the overall differential attenuation coefficient due to absorption and scattering, and $w(z)$ is the spot-size function. Note that the input lens L2 focuses the beam to a waist radius of $w_0$ which was 25 μm in the experiments. Furthermore, the maximum value of $w(z)$ within the cuvette (320 μm) was much smaller than the width of the cuvette (10 mm). Hence, the total power of the beam can be calculated by assuming that the cross-sectional size of the medium is infinite in extent, in comparison with the beam size, leading to the following expression for the beam power within the solution:

$$P(z)=\int_0^{2\pi}d\theta\int_0^{\infty}drrI(r,z)=P_0\exp(-\alpha z)\,. \qquad (2)$$

Hence, the power $P_A$ lost due to attenuation within the cuvette and the transmitted power $P_t$ become $P_A=P_0(1-\exp(-\alpha L))$ and $P_t=P_0\exp(-\alpha L)$, respectively, where $L$ is the

length of the cuvette (Fig. 1(b)). In the analysis of the conversion efficiencies, $P_A$ was determined from the experimentally measured values of the incident ( $P_i$ ), reflected ( $P_r$ ), and transmitted ( $P_t$ ) powers by using

$$P_A = P_i - P_r - P_t . \qquad (3)$$

Returning to the heating problem, we assume that the system, consisting of the cuvette and the nanoparticle solution with respective masses of $m_c$ and $m_s$, and specific heat capacities of $c_c$ and $c_s$, can be modelled as a lumped element. The net heat energy $dQ$ delivered to the system (cuvette plus the nanoparticle solution) will then result in a temperature change $dT$ given by

$$dQ = \left(m_c c_c + m_s c_s\right) dT . \qquad (4)$$

The time rate of change $dQ/dt$ of the net heat delivered to the system can then be expressed as

$$\frac{dQ}{dt} = \left(m_c c_c + m_s c_s\right)\frac{dT}{dt} = P_H - \kappa_C \left[T(t) - T_0\right] - \kappa_R \left[T(t)^4 - T_0^4\right], \qquad (5)$$

where $P_H$ is the effective heating power of the solution, $T(t)$ is the absolute temperature of the cuvette, and $T_0$ is the ambient absolute temperature. In addition, $\kappa_C$ and $\kappa_R$ represent the convective and radiative heat transfer coefficients of the cuvette containing the nanoparticle solution. Noting that

$$\left[T(t)^4 - T_0^4\right] = \left[T(t) - T_0\right]\left[T(t)^3 + T(t)^2 T_0 + T(t) T_0^2 + T_0^3\right], \quad (6)$$

Eq. (2) can be rewritten as

$$\left(m_c c_c + m_s c_s\right)\frac{dT}{dt} = P_H - \kappa(T)\left[T(t) - T_0\right], \qquad (7)$$

where $\kappa(T)$ is the effective temperature-dependent heat transfer coefficient given by [84]

$$\kappa(T) = \kappa_C + \kappa_R \left(T^3 + T^2 T_0 + T T_0^2 + T_0^3\right). \qquad (8)$$

Strictly speaking, $\kappa(T)$ is temperature dependent as can be seen from Eq. (8) and no explicit analytical solution of Eq. (5) exists to the authors' knowledge. However, if the maximum temperature rise $\Delta T_{\max}$ is small compared to $T_0$, $\kappa(T)$ given by Eq. (8) remains nearly constant at $\kappa(T_0)$ and the time evolution of the temperature can be determined analytically from the solution of the linearized model given in Eq. (7). In the specific example provided here, using about 0.9 g of $Ag_2S$-GSH QD solution at 5mg/mL concentration, the total incident pump power at each wavelength was kept at 200 mW, resulting in measured $\Delta T_{\max}$ of less than 15 K and a corresponding $\Delta T_{\max}/T_0$ value of about 5%. In this case, the radiative contribution to $\kappa(T)$ (the bracketed term in Eq. (8)) varies by no more than 8%, hence justifying the use of the linearized model (in other words, Eq. (7) with a constant heat transfer coefficient $\kappa(T_0)$) for temperature calculations. To emphasize again, we are not neglecting the radiative cooling of the cuvette. Rather, we are assuming that both radiative and convective heat transfer obey a linear model. Determination of the convective and radiative components of $\kappa(T)$ in this regime was not possible, nor was it necessary for the calculation of the photothermal conversion efficiencies. Such a task would require larger temperature rises so that the $T^4$ contribution to radiative cooling is not negligible and was beyond the scope of this work.

When $\kappa(T)$ is assumed to be constant at $\kappa(T_0)$, Eq. (7) can be readily solved, yielding

$$T(t) = T_{\max} + (T_0 - T_{\max})\exp\left(-\frac{t}{\tau_h}\right), \qquad (9)$$

where $\tau_h$ is the characteristic heating time related to $\kappa(T_0)$ via

$$\tau_h \kappa(T_0) = m_c c_c + m_s c_s \qquad (10)$$

and $T_{\max}$ is the maximum temperature attained by the system. By using the particular solution of Eq. (7), $P_H$ can be determined in terms of $T_{\max}$ from

$$P_H = \kappa(T_0)(T_{\max} - T_0) = \frac{m_c c_c + m_s c_s}{\tau_h}(T_{\max} - T_0). \qquad (11)$$

If we further assume that the pure solution without the nanoparticles also has some absorption at the laser wavelength, giving rise to a heating power $P_{Hs}$ and a corresponding maximum temperature rise $T_s$, satisfying

$$P_{Hs} = \frac{m_c c_c + m_s c_s}{\tau_h}(T_s - T_0), \qquad (12)$$

then the effective heating power $P_{Hn}$ of the nanoparticles will simply be $P_{Hn} = P_H - P_{Hs}$.

At this point, we introduce two different heating efficiencies to quantify the efficiency of heating induced by the nanoparticles: the intrinsic conversion efficiency $\eta_i$ and the external conversion efficiency $\eta_{ext}$. The efficiencies $\eta_i$ and $\eta_{ext}$ are defined respectively as

$$\eta_i \equiv \frac{P_{Hn}}{P_A} = \frac{\left(m_c c_c + m_s c_s\right)}{\tau_h P_i \left(1-R-T\right)}\left[\left(T_{\max} - T_0\right) - \left(T_s - T_0\right)\right] \qquad (13)$$

and

$$\eta_{ext} \equiv \frac{P_{Hn}}{P_i} = \frac{\left(m_c c_c + m_s c_s\right)}{\tau_h P_i}\left[\left(T_{\max} - T_0\right) - \left(T_s - T_0\right)\right]. \qquad (14)$$

Above, $R = P_r / P_i$ and $T = P_t / P_i$ are the experimentally measured power reflection and power transmission coefficients for the cuvette-solution system (see Fig. 1(b) for the description of $P_r$ and $P_t$ ). The intrinsic conversion efficiency $\eta_i$ gives the fraction of the absorbed laser power that is converted into heating power by the nanoparticles, whereas the external conversion efficiency $\eta_{ext}$ gives the fraction of the incident optical power converted to heating power. Generally, $\eta_{ext}$ is smaller than $\eta_i$ due to the finite reflectance of the input surface of the cuvette and the finite absorption of the solution. Even if the nanoparticle concentration and cuvette length are adjusted to make the absorption nearly 100%, the surface reflectance may not be negligible. This point also deserves attention during *in vivo* experiments, where surface scattering can cause further reduction of the optical power coupled to the tissue.

# CHAPTER 4:
# RESULTS AND DISCUSSION

## *4.1 In vitro Experimental Results*

### *4.1.1 Results of $Ag_2S$-GSH QDs*

Figure 4.1 shows a representative heating curve and the thermal image of the cuvette, when the steady-state maximum temperature was reached (approximately after 30 min of irradiation). In this particular case, the laser operated at the wavelength of 780 nm. The incident, reflected, and transmitted powers were 215, 15, and 26 mW, respectively. The maximum temperature rise of the solution was determined by averaging the temperature distribution over the exit window of the cuvette (shown as the rectangular box ABCD in Figure 4.1(b). For this specific case, the maximum temperature rise averaged over the box ABCD came to 14.2 °C, about 1.8 °C lower than the maximum temperature recorded with the thermocouple. Averaged maximum temperature rise ($\Delta T_{max}$) data determined from thermal camera measurements were used in the calculation of photothermal conversion efficiencies, as described in chapter 3. Similar data obtained at different laser wavelengths are shown in Appendix A.

.

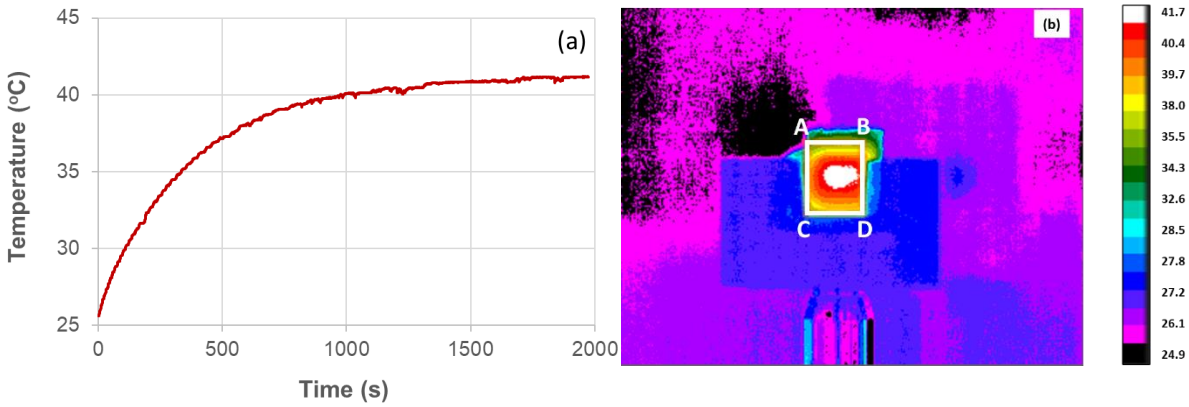


Figure 4.1. (a) Measured time-dependent heating curve recorded with the thermocouple and (b) the resulting steady-state IR camera image of the PAA/SPION solution.

As measurements were taken by varying $Ti^{+3}$-sapphire wavelength in 10 nm steps between 720-810 nm. Below are the other heating curves at 730 nm,750 nm, 800 nm and their corresponding thermal camera images.

The time-dependent heating curve of pure water recorded between 730-810 nm with the thermocouple. One representative heating curve at the wavelength of 750 nm is in the Figure 4.2. The laser power coupled to the cuvette ($P_0 = P_i - P_r$) was kept at 200 mW. Note that prior to laser irradiation, which started at time $t_1$ in Figure 4.2a, there was an initial 0.3 °C drift in the temperature before the initial steady-state temperature was reached. Such an initial drift was observed in all pure water measurements and was used to estimate our error in temperature measurements. By repeating the initial temperature drift measurement for nine different cases, the error in our temperature measurements was estimated to be 0.37 °C. At time $t_1$, the image of the cuvette was recorded with the thermal camera (see Figure 4.2b), laser irradiation was started, and the camera was then turned off. After the next steady state was reached under laser irradiation, corresponding to time $t_2$ in Figure 4.2a, the thermal camera was turned on again to capture the final steady-state temperature distribution of the cuvette (Figure 4.2c). Between $t_1$ and $t_2$, the thermal camera was kept off to minimize additional sources of heat other than laser irradiation since the temperature rise for pure water is very small. In addition, the cuvette setup was kept inside a plexiglass box to minimize air currents during delicate temperature measurements. Based on the thermal camera images shown in Figure 4.2 b,c, the maximum averaged temperature rise of pure water was measured as 0.60 °C at the wavelength of 750 nm. The measured maximum temperature rise at different laser wavelengths was then averaged to yield an estimated maximum temperature rise of 0.58 °C for pure water. The use of an average temperature rise for pure water is justified by the fact that the measured absorbance of the cuvette−pure water combination was approximately constant over the 720− 810 nm spectral window. Data similar to Fig. 4.2, taken at different wavelengths are shown in Appendix B.

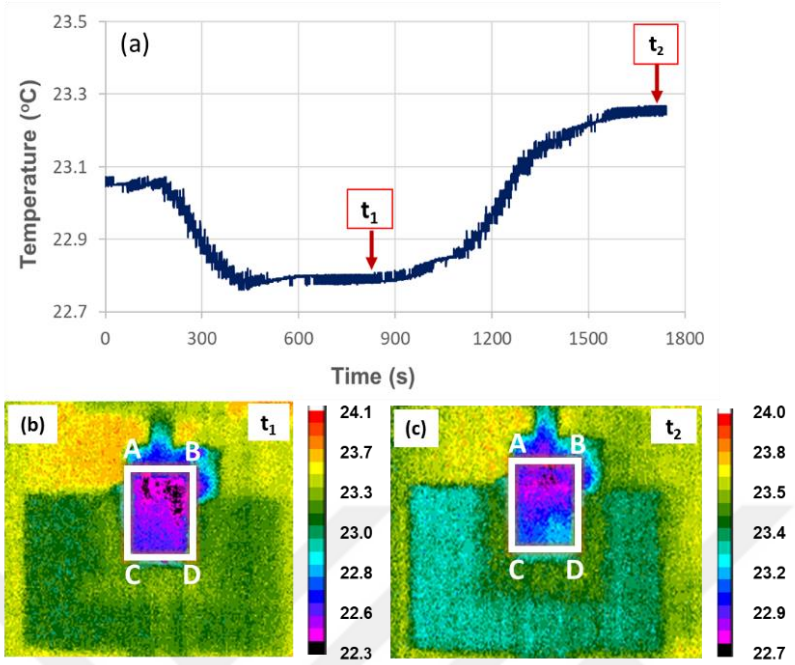


Figure 4.2 (a) Time-dependent heating curve recorded with the thermocouple for pure water at the wavelength of 750 nm, (b) thermal camera image of the cuvette at time $t_1$, and (c) thermal camera image of the cuvette at time $t_2$.

Figure 4.3 shows the power reflectivity $R = P_r/P_i$ of the solution-filled cuvette was nearly constant at about 7% over the 720−810 nm wavelength range, whereas the power transmission ($T = P_t/P_i$) monotonically increased from 4.2% at 720 nm to 19.5% at 810 nm due to the decrease of the absorbance of the nanoparticle solution with wavelength. Figure 4.3 a,b shows the measured power reflectivity (R) of the cuvette and the absorption $A = 1 - T - R$ of the $Ag_2S$-GSH QD solution (concentration of 5 mg/mL).

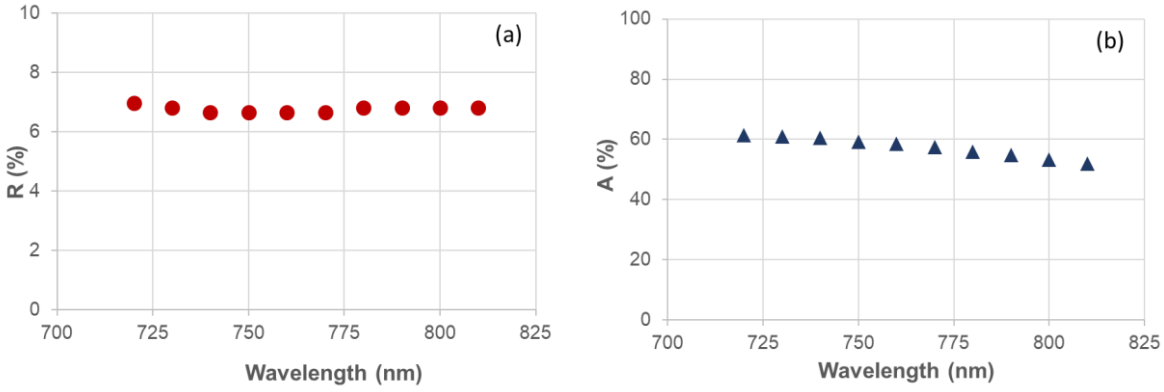

Figure 4.3 Measured (a) power reflectivity R of the cuvette, (b) absorption A = 1 − T − R of the $Ag_2S$-GSH QD solution over the 720− 810 nm range. All equations in this discussion are referring to in chapter 3 equations. Equation 13 was used to determine the intrinsic conversion efficiency $\eta_i$ of the $Ag_2S$-GSH QDs. Here, the analytical solution of the heating problem given by eq 9 in chapter 3 was fit to each measured time-dependent heating curve to extract the value of the characteristic heating time $\tau_h$. As an example, Figure 5a shows one set of measured and fit time-dependent heating data at 780 nm irradiation measured with the thermocouple. The solution was heated for approximately 30 min until a steady-state temperature was reached. The temperature data were collected after each second. Fewer experimental data points are displayed in Figure 4.4a so that the fitting curve can be clearly seen. Overall, very good fits could be obtained between T(t) given by eq 9 in previous chapter and the experimentally measured heating data. To minimize the measurement error, three sets of heating data were obtained at each laser wavelength, using a fresh $Ag_2S$-GSH QD solution as well as a new cuvette for each set. Figure 4.4b shows the average heating time at different laser irradiation wavelengths between 720 and 810 nm. $\tau_h$ varied between 335 and 390 s, with an average of 358 s.

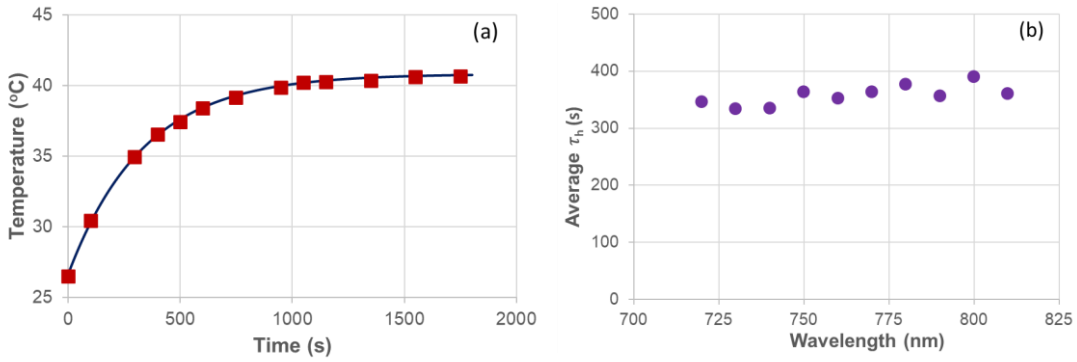


Figure 4.4 (a) Representative graph showing the measured and fit variation of the temperature for the Ag2S-GSH QD solution as a function of time under 750 nm irradiation and (b) variation of the best-fit heating time, averaged over three measurements at each irradiation wavelength between 720 and 810 nm

Figure 4.5 shows the measured maximum temperature rise (($T_{max} - T_0$) appearing in eq 13) of the $Ag_2S$-GSH QD solution (concentration of 5 mg/mL) as a function of laser wavelength, averaged over three sets of measurements at each wavelength. Equations 13 and 14 were used in the determination of the intrinsic and external heating efficiencies.

The average measured value of 0.58 °C was used for the maximum temperature rise ($T_s - T_0$) of pure water at each laser wavelength. Two sources of error were identified in the efficiency calculations: error of $\delta T = 0.37$ °C in temperature measurements and 5% error in power measurements, leading to an overall error margin of ±2.8% in efficiency measurements, based on standard error propagation analysis.

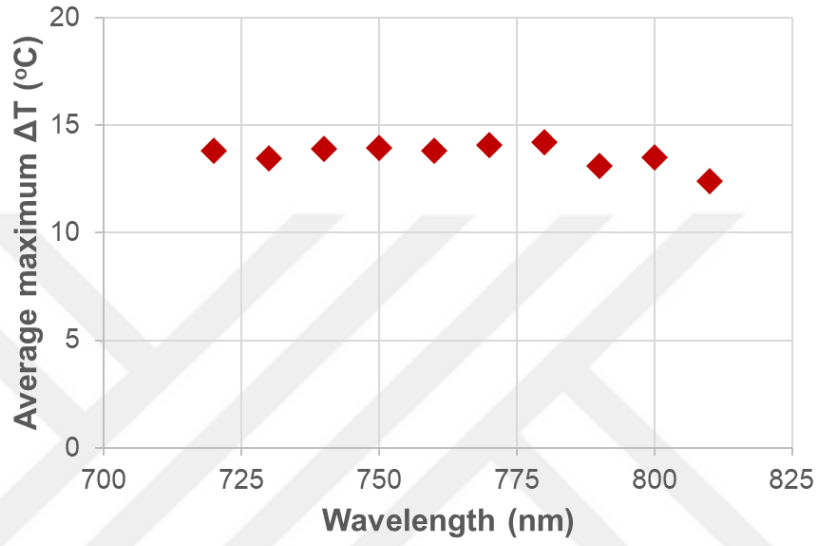


Figure 4.5 Averaged maximum temperature rise of the $Ag_2S$-GSH QD solution measured with the thermal camera at different wavelengths between 720 and 810 nm.

Figure 4.6a shows the average measured intrinsic photothermal conversion efficiency $\eta_i$ as a function of irradiation wavelength for the $Ag_2S$-GSH QDs between 720 and 810 nm. The results based on the analysis described in chapter 3 show that $\eta_i$ is high for these nanoparticles ranging between 91 and 96% in this wavelength range. In the case of the external conversion efficiency $\eta_{ext}$, there is a monotonic decrease of the conversion efficiency from 82 to 70% in the 720−810 nm wavelength window. The reduction in external conversion efficiency with increasing wavelength primarily stems from the wavelength dependent absorption. We note in passing that low input powers around 200 mW were preferred in this experiment to limit the maximum temperature rise so that the linearized model could be used in the analysis of the experimental heating data. By increasing the incident power or reducing the sample size, higher temperature rise can be achieved, as was demonstrated in our earlier PTT experiments with $Ag_2S$-GSH QDs.

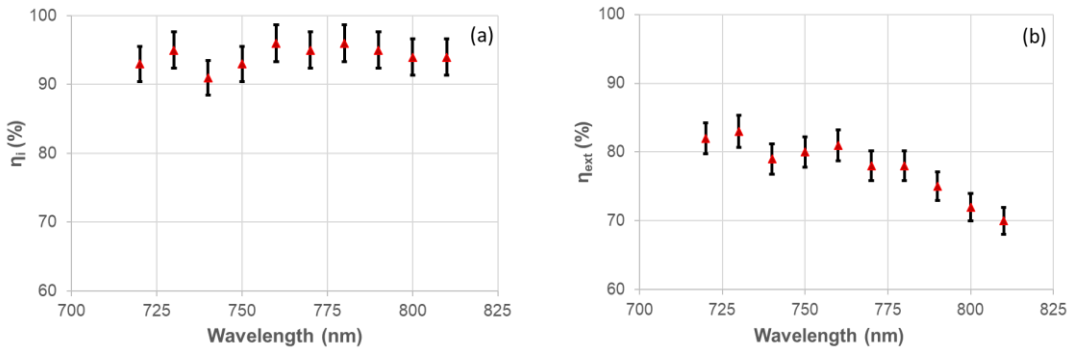


Figure 4.6 Measured (a) intrinsic ($\eta_i$) and (b) external ($\eta_{ext}$) photothermal conversion efficiency of AgS2-GSH QD solution between 720 and 810 nm.

### *4.1.2 Results of PAA-SPIONS*

The measured time dependent heating curve recorded with the thermocouple and the resulting steady-state IR camera image of the PAA/SPION solution are shown in Figure 4.7a, b, respectively. The heating time averaged over six measurements came to 355 s. The average intrinsic and external efficiencies of the PAA/SPIONs were determined to be 83.4 and 73.4%, respectively, at 810 nm. The standard deviation in the efficiency values was 0.6%, indicating that the method proposed in this study is highly repeatable.

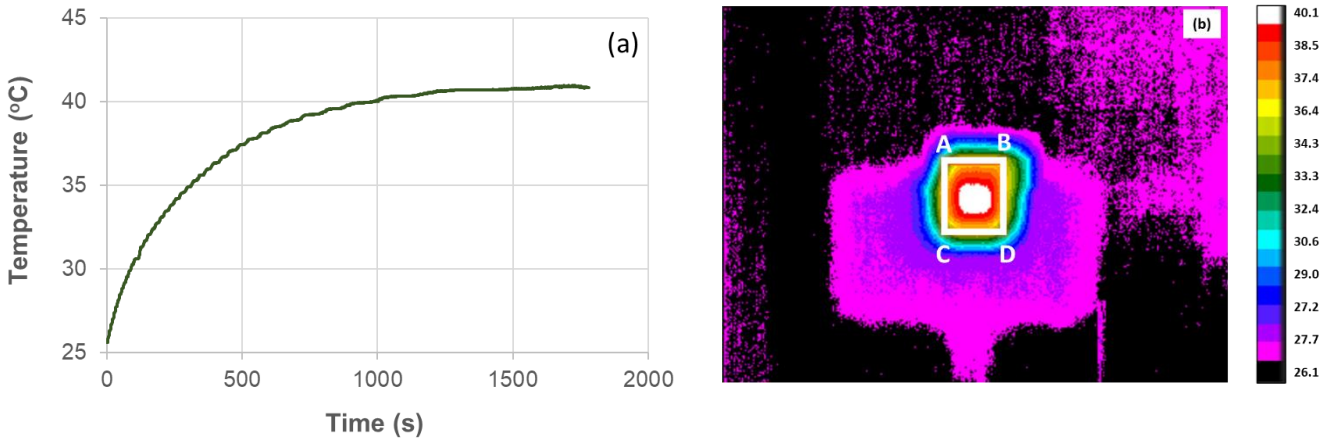


Figure 4.7 (a) Measured time-dependent heating curve recorded with the thermocouple and (b) the resulting steady-state IR camera image of the PAA/SPION solution.

### *4.1.3 Results of at 640 nm*

To demonstrate the solution-set up working and resultant efficiency polyacrylic acid coated superparamagnetic iron oxide (PAA-$Fe_3O_4$) was irradiated with 640 nm fiber coupled diode laser for approximately thirty minutes. The resultant heating curve and its corresponding FLIR camera image that is displayed in figure 4.8a,b. The incident reflected and transmitted powers were 215, 08, 76 mW respectively. The average temperature increase measured within the area shown (figure 4.8(b)) in thermal camera images with a square box ABCD was 10.3℃ while thermocouple measured localized temperature increase was comparatively 3.2℃ higher. Time constant ($\tau_h$) was measured to be 389s. Average solution mass was 0.722 g. By inserting all the experimental results into the equation 13 and 14 in chapter 3, we found intrinsic and extrinsic efficiency of this nanoparticle to be 76% and 63%.

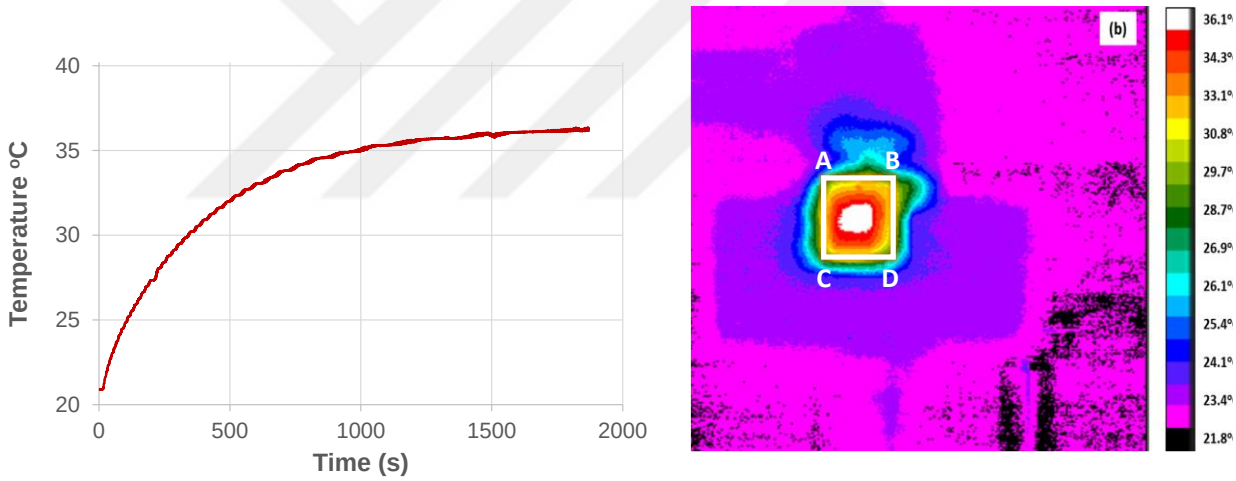


Figure 4.8 (a) PAA-$Fe_3O_4$ time dependent heating curves at 640 nm (b) the resulting steady-state IR camera image of the PAA-$Fe_3O_4$ solution.

## *4.2 In vivo Experimental Results*

Four mice were taken for the experiment. One mouse that was only injected with 10 mg/kg $Ag_2S$-GSH-Herceptin QDs that reached 39.6 ℃ after 10 minutes of laser irradiation and room temperature was 25.8 ℃. The body temperature increase was 6.2 ℃. Figure 4.9 (a, b, c) shows temperature increase by FLIR camera over time.

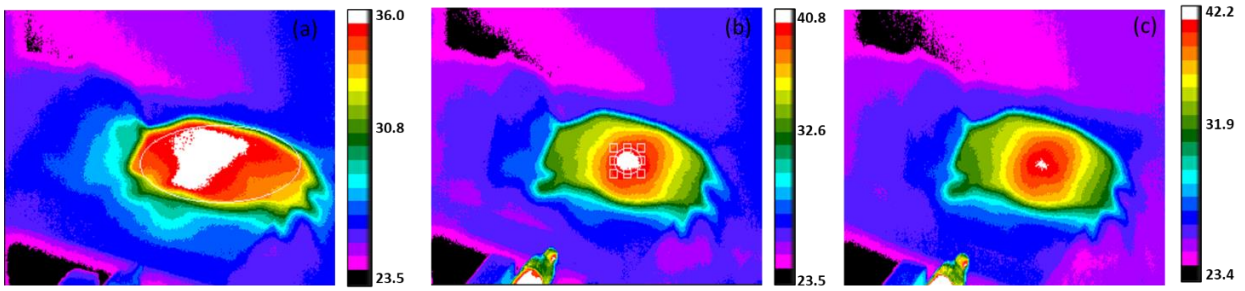


Figure 4.9: IR camera image for subcutaneously injected mouse with 10 mg/kg $Ag_2S$-GSH QDs (a) without irradiation (b) 5 minutes of irradiation (c) 10 minutes of irradiation

The second mouse was also injected with 10 mg/kg of $Ag_2S$-GSH-Herceptin but along with Cisplatin. Temperature reached up to 41.6 ℃ while room temperature was 27 ℃. So, 6.2 ℃ temperature increase was observed with respect to body temperature. The temperature variations over the time in Figure 4.10 indicate that Cisplatin is not playing any role in temperature rise.

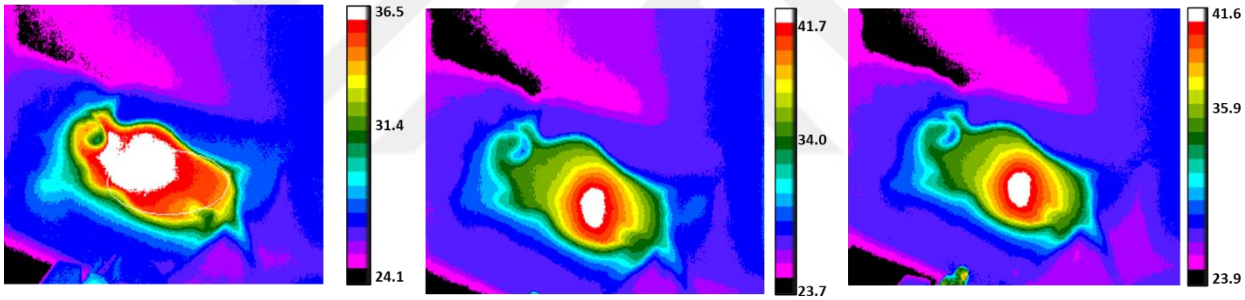


Fig 4.10: IR camera image for subcutaneously injected mouse with 10 mg/kg $Ag_2S$-GSH-Herceptin QDs and Cisplatin (a) without irradiation (b) 5 minutes of irradiation (c) 10 minutes of irradiation.

Another set of experiments was performed with the mentioned set-up and parameters with a different QD concentration (20 mg/kg of QDs) with and without Cisplatin (Figure 4.11 and 4.12). The mice were injected subcutaneously 24 h before laser treatment. The temperature in the animal with QD-Cisplatin was increased from 30.2 ℃ to 39.6 ℃ whilst the temperature enhanced from 34.3 to 43.5 ℃ in the animals treated with only QDs. The reason attributes to the fact that high absorbance of the QDs at NIR region could cause temperature increase upon irradiation while cisplatin lacks absorbance at 808 nm. This

clearly demonstrates that the major heating comes from QDs that would lead to mild hyperthermia.

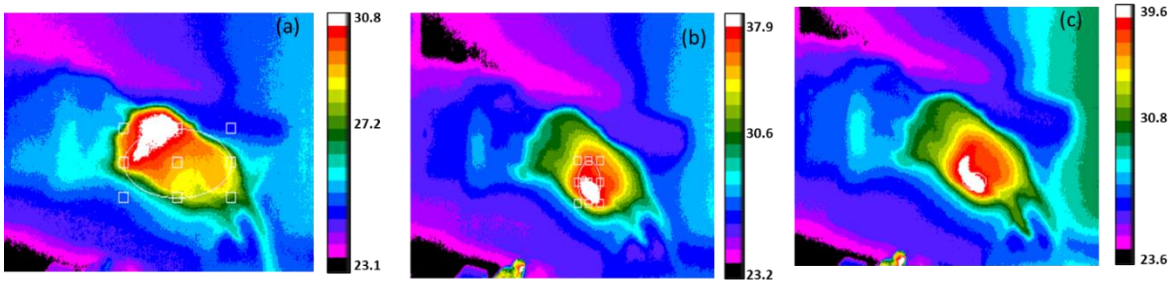


Figure 4.11: IR camera image for subcutaneously injected mouse with 20 mg/kg $Ag_2S$-GSH-Herceptin QDs (a) without irradiation (b) 5 minutes of irradiation (c) 10 minutes of irradiation.

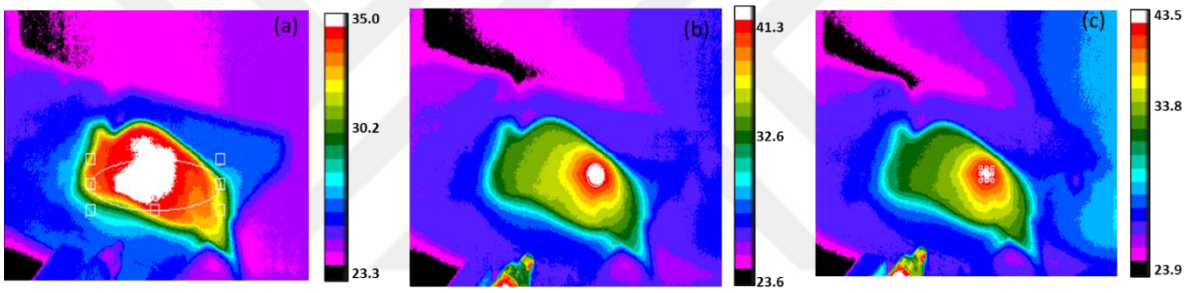


Figure 4.12: IR camera image for subcutaneously injected mouse with 20 mg/kg $Ag_2S$-GSH-Herceptin QDs and Cisplatin (a) without irradiation (b) 5 minutes of irradiation (c) 10 minutes of irradiation.

Furthermore, to investigate the effect of laser intensity within the safe range on temperature rise, the intensity was increased from 1.48 W/cm$^2$ to 1.59 W/cm$^2$. The 20 mg/kg dose was injected in a mouse subcutaneously 24 h prior to the laser irradiation. As shown in Figure 4.13, the temperature improved from 31.6$^o$C to 47.5$^o$C ($\Delta T$ = ~15$^o$C) at 1.59 W/cm$^2$. In general, higher power intensity enhances the delta-T. However, it may cause irritation, redness, and other side effects in the mice after laser treatment. To make sure that increase in the laser intensity did not cause any significant side effects, animals were monitored for 14 days after PTT. No symptoms of burn, dehydration, and weight loss were observed after 14 days.

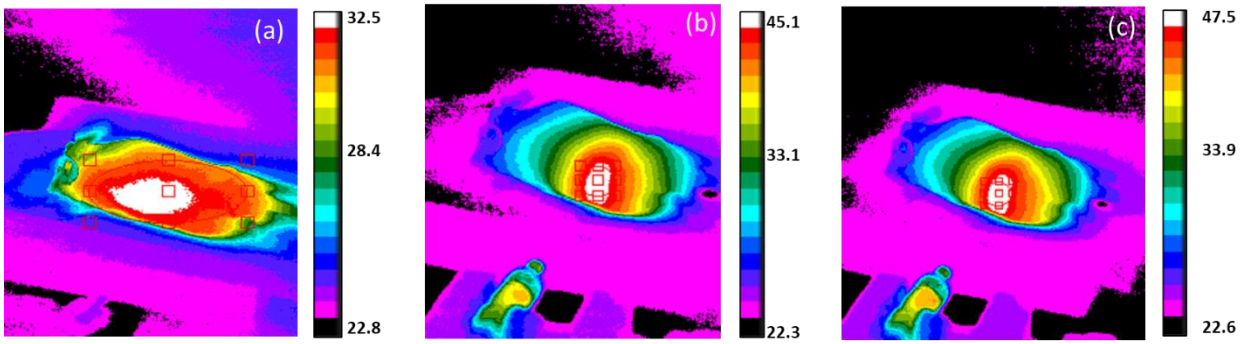


Figure 4.13: IR camera images of mouse irradiated with 1.59 W/cm$^2$ (a) without irradiation (b) 5 minutes of irradiation (c) 10 minutes of irradiation.

QDs were administered to the mice intratumorally, intravenously, and subcutaneously. Animals that received QDs subcutaneously showed higher temperature increase compared to the others. Since the size of the tumors were small, lower nanoparticles were injected to the mice intratumorally. Therefore, the $\Delta T$ was observed less than expected amount resulting due to the lower concentration of QDs in the site of tumors. In the case of intravenous injection, due to the distribution of nanoparticles in the other organs, the final concentration of QDs in the tumor were less than subcutaneous injection causing lower temperature to increase after PTT.

# CHAPTER 5:
# CONCLUSION

We presented an accurate experimental method for the determination of the photothermal conversion efficiency of nanoparticles in solution. Two different photothermal conversion efficiencies, namely, intrinsic and external conversion efficiency, were introduced to relate the induced heating power of the nanoparticles to the absorbed and incident laser power, respectively. Measurement of the maximum temperature rise was performed using an infrared camera, where averaging over the cuvette surface minimizes the measurement error due to the specific positioning of the thermocouple inside the solution. The model used in the analysis of the data was also reviewed, and explicit formulas were provided for the calculation of the intrinsic and external conversion efficiencies in terms of the parameters measured in the experiments. The method was applied to $Ag_2S$-GSH QDs, and a tunable Ti3+:sapphire laser was used to investigate the variation of efficiency over the 720−810 nm wavelength range. The results show that the intrinsic photothermal conversion efficiency of $Ag_2S$-GSH QDs was very high, exceeding 91% over this spectral window, making these quantum dots especially suitable for photothermal therapy applications with near-infrared laser irradiation. This approach was also adopted to PAA/SPIONs, which have become quite popular as PTT agents in recent years. The average intrinsic and external efficiencies of the PAA/SPIONs were determined to be 83.4 and 73.4%, respectively, at 810 nm. The intrinsic and extrinsic efficiency measured for PAA/SPIONs with 600 μg/ml concentration of Fe came out to be 76% and 63% at 640 nm. We expect that the systematic experimental approach described in this thesis should prove useful for the evaluation of a wide variety of potential nanoparticles for photothermal therapy applications.

After extensive study of photothermal conversion efficiency of $Ag_2S$-GSH Herceptin QDs were injected into the tumor SKBR3 bearing nude mice. The QDs were injected subcutaneously, intratumorally and intravenously and temperature rise was observed with well calibrated FLIR camera. In this thesis, we discussed results of subcutaneously injected QDs. Two dozes 10 mg/kg and 20 mg/kg of $Ag_2S$-GSH Herceptin were studied at 1.49 W/cm$^2$ with and without cisplatin. Temperature increase of only QDs was 6.2℃ for 10 mg/kg of doze with and without Cisplatin and for 20 mg/kg temperature increase

was ~9℃ for both only QDs and with Cisplatin. It was obvious that cisplatin has insignificant absorption at 793 nm. When the laser intensity was increased from 1.49 W/cm$^2$ to 1.59 W/cm$^2$ and applied for 10 minutes on a mouse, the temperature rise was measured as 15℃.

# Appendix A. Heating curves and their corresponding FLIR camera images between 720-810 nm

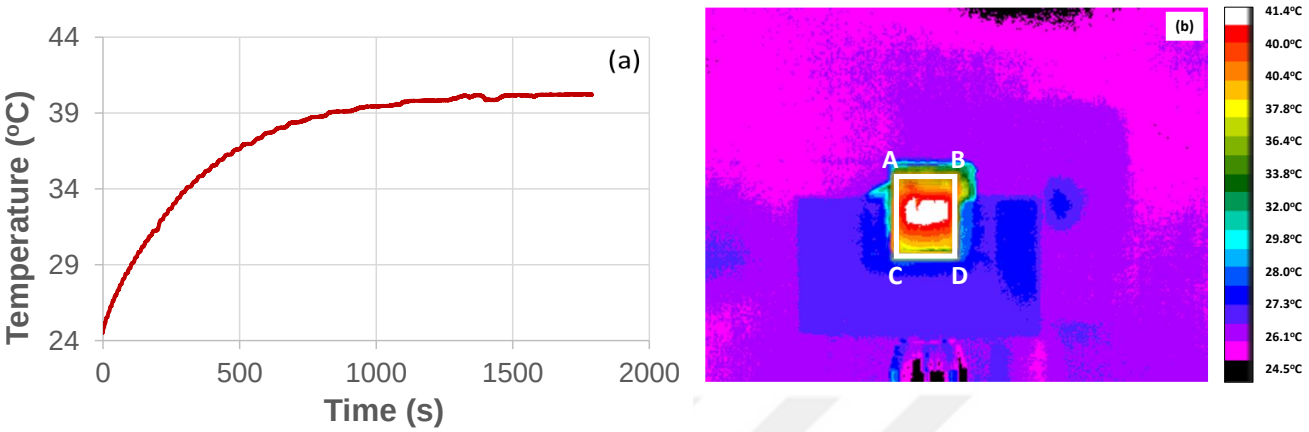


Figure A-1 (a) Measured time-dependent heating curve recorded with the thermocouple at 720 nm and (b) the resulting steady-state IR camera image of the PAA/SPION solution at 720 nm.

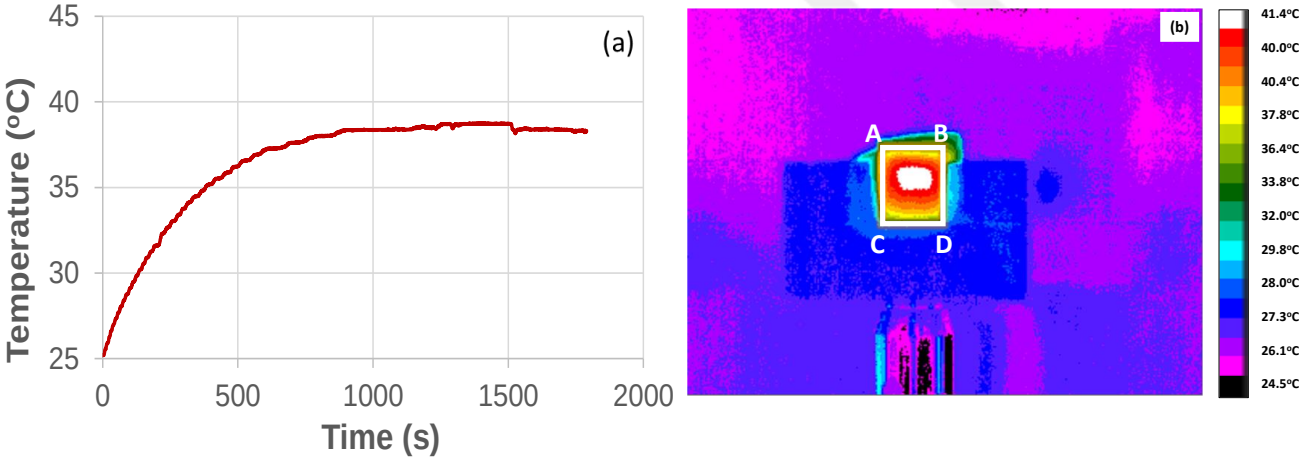


Figure A-2 (a) Measured time-dependent heating curve recorded with the thermocouple at 730 nm and (b) the resulting steady-state IR camera image of the PAA/SPION solution at 730 nm.

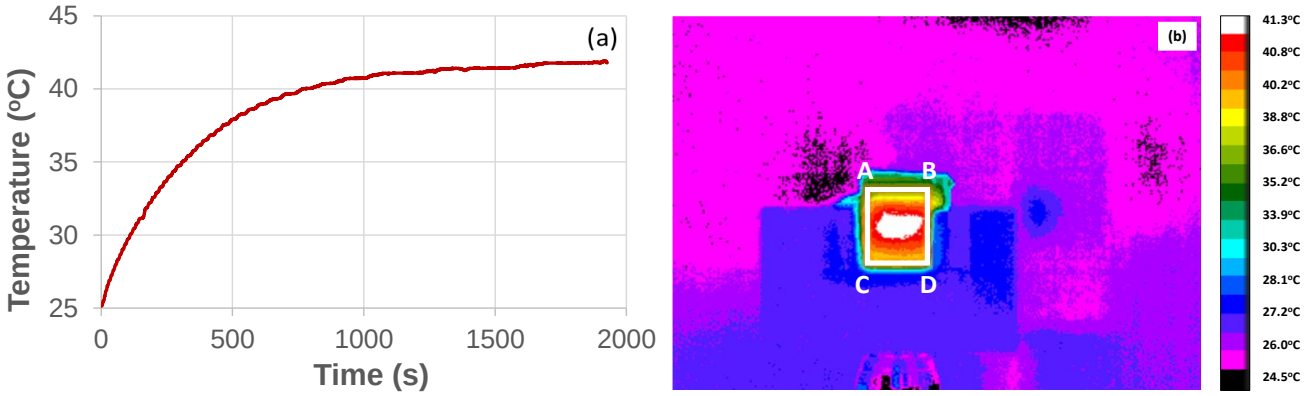


Figure A-3 (a) Measured time-dependent heating curve recorded with the thermocouple at 740 nm and (b) the resulting steady-state IR camera image of the PAA/SPION solution at 740 nm.

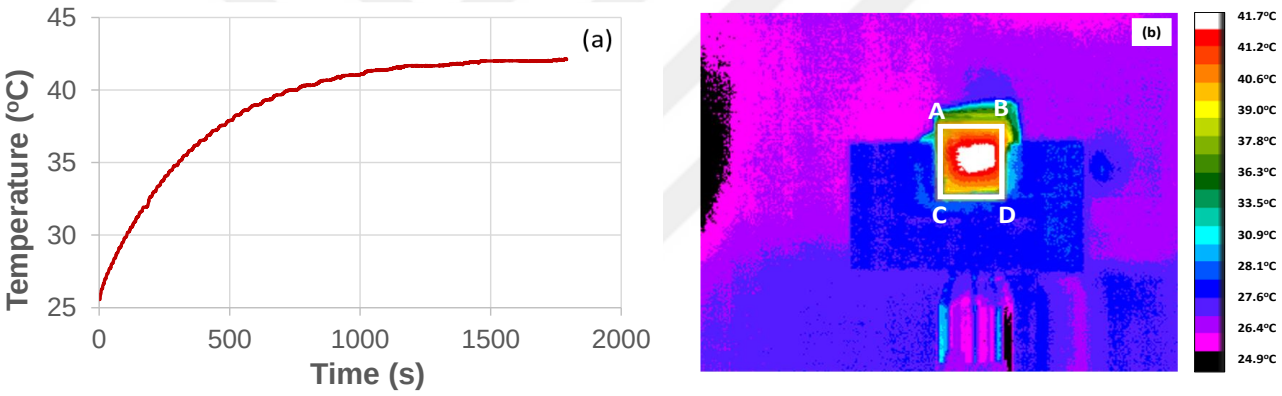


Figure A-4 (a) Measured time-dependent heating curve recorded with the thermocouple at 750 nm and (b) the resulting steady-state IR camera image of the PAA/SPION solution at 750 nm

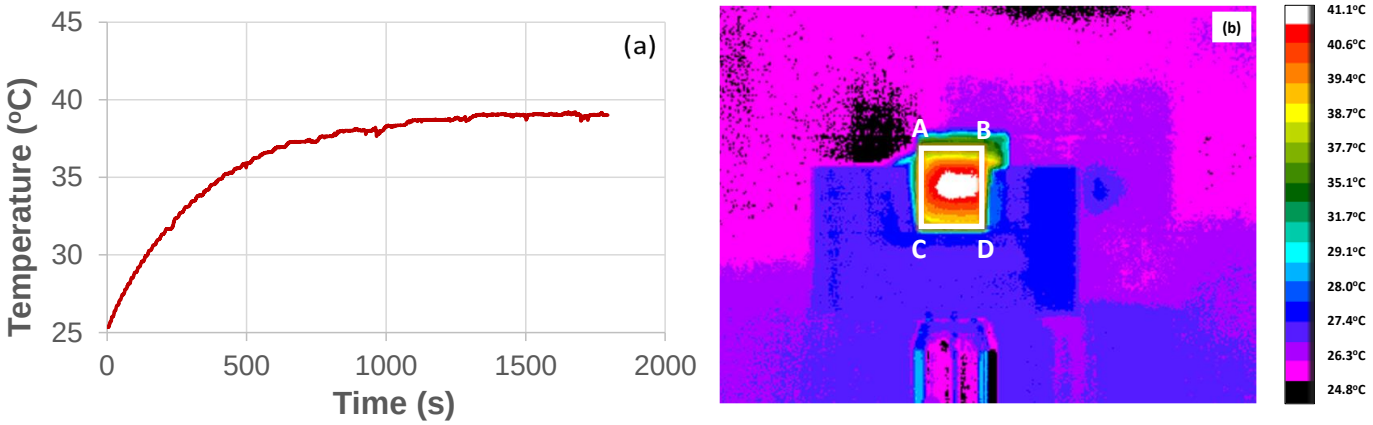

Figure A-5 (a) Measured time-dependent heating curve recorded with the thermocouple at 760 nm and (b) the resulting steady-state IR camera image of the PAA/SPION solution at 760 nm

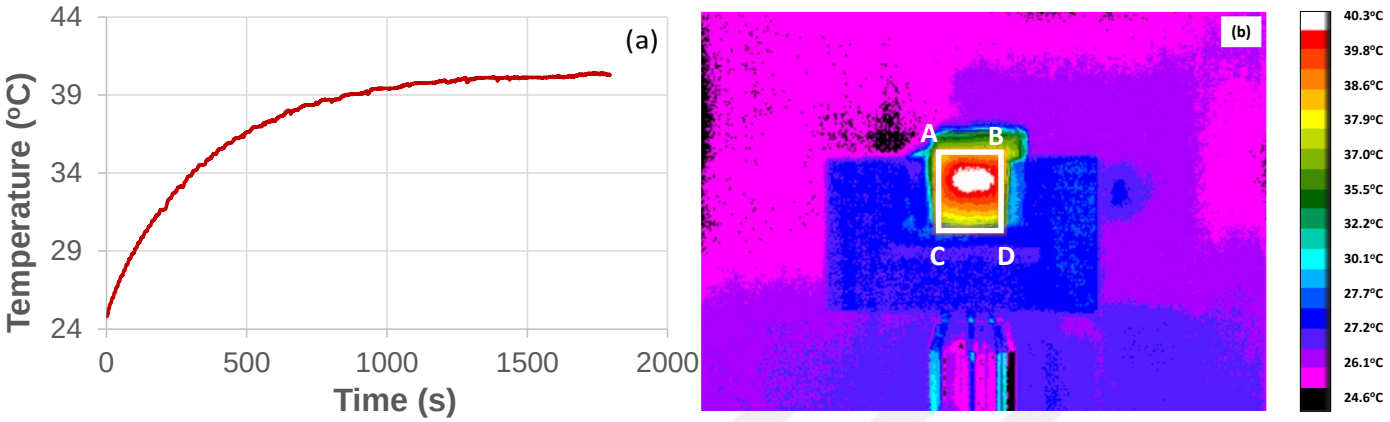


Figure A-6 (a) Measured time-dependent heating curve recorded with the thermocouple at 770 nm and (b) the resulting steady-state IR camera image of the PAA/SPION solution at 770 nm

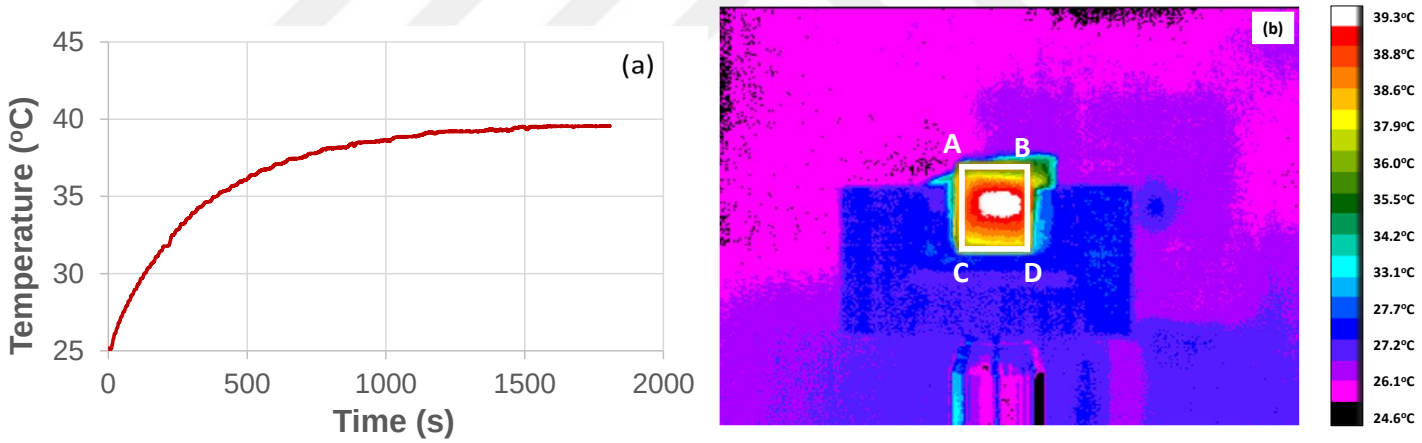


Figure-A-7 (a) Measured time-dependent heating curve recorded with the thermocouple at 790 nm and (b) the resulting steady-state IR camera image of the PAA/SPION solution at 790 nm

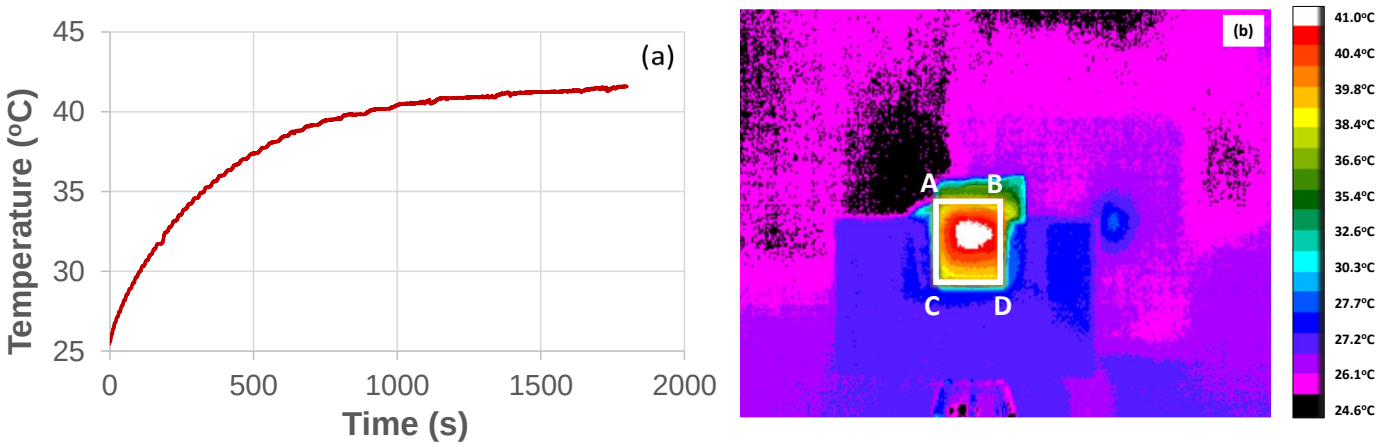


Figure-A (a) Measured time-dependent heating curve recorded with the thermocouple at 800 nm and (b) the resulting steady-state IR camera image of the PAA/SPION solution at 800 nm

# Appendix B: **TIME-DEPENDENT HEATING CURVE RECORDED WITH THE THERMOCOUPLE FOR PURE WATER AND THERMAL CAMERA IMAGE AT 770 AND 790 NM**

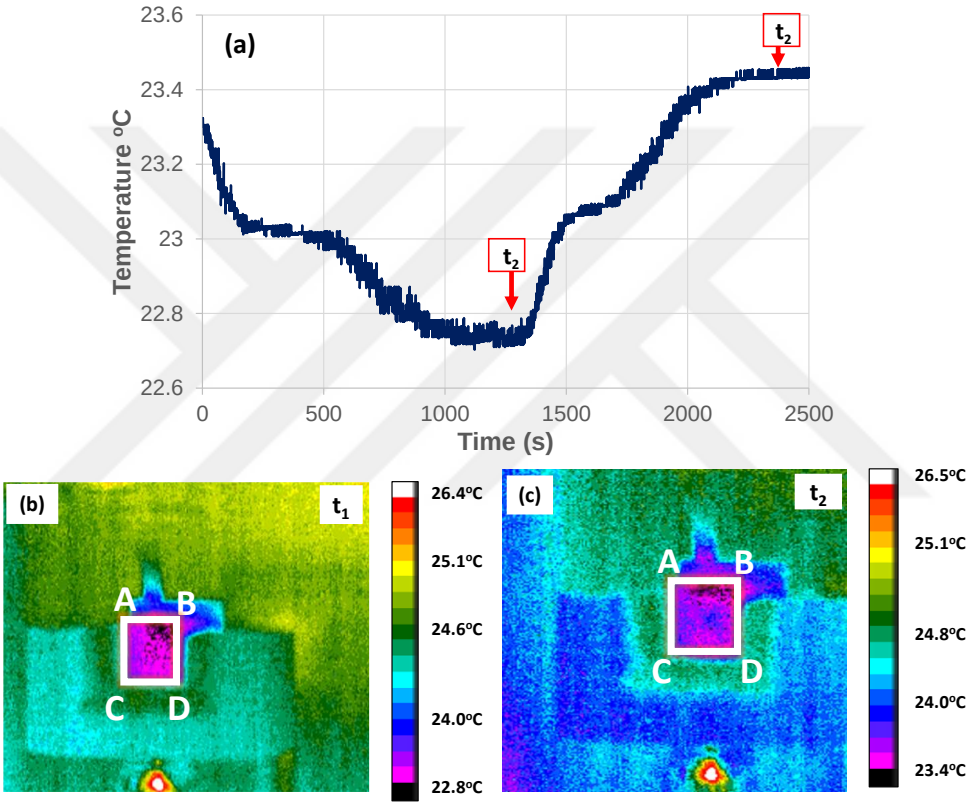


Figure B-1 (a) Time-dependent heating curve recorded with the thermocouple for pure water at the wavelength of 770 nm, (b) thermal camera image of the cuvette at time $t_1$, and (c) thermal camera image of the cuvette at time $t_2$**.**

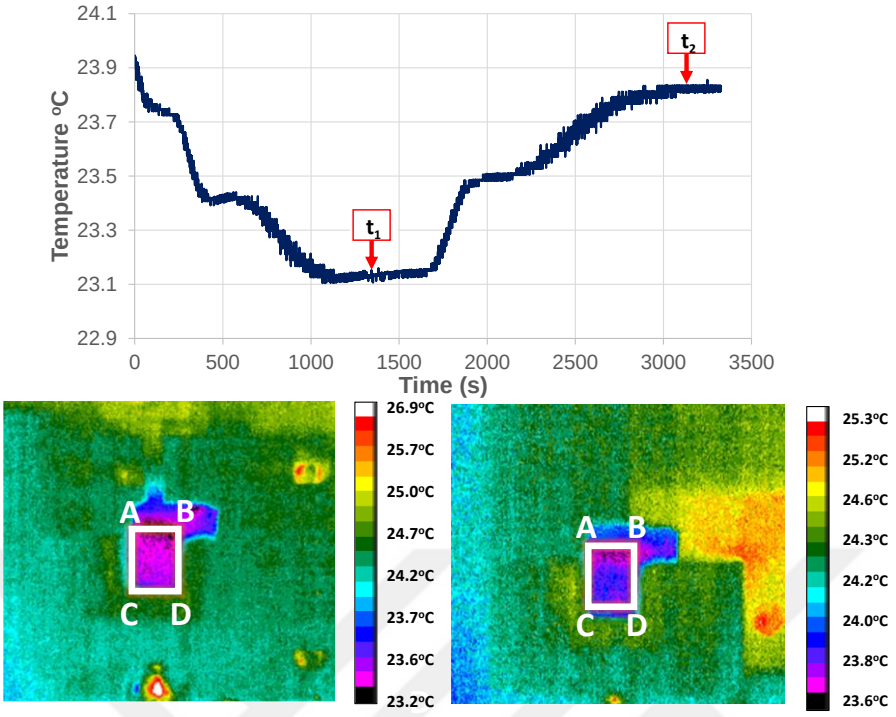


Figure B-2 (a) Time-dependent heating curve recorded with the thermocouple for pure water at the wavelength of 790 nm, (b) thermal camera image of the cuvette at time $t_1$, and (c) thermal camera image of the cuvette at time $t_2$.

# BIBLIOGRAPHY

[1] N. Gupta, "ANCIENT LIGHT THERAPIES: A BOON TO MEDICAL SCIENCE," *Science and culture*, vol. 82, 07/13 2018.

[2] P. K. Gupta and H. S. Patel, "Biomedical Applications of Lasers," in *Laser Physics and Technology*, New Delhi, P. K. Gupta and R. Khare, Eds., 2015// 2015: Springer India, pp. 301-331.

[3] H. Jelínková, *Lasers for medical applications: diagnostics, therapy and surgery*. Elsevier, 2013.

[4] L. R. Solon, R. Aronson, and G. Gould, "Physiological implications of laser beams," *Science*, vol. 134, no. 3489, pp. 1506-1508, 1961.

[5] D. S. Choy, "History of lasers in medicine," (in eng), *Thorac Cardiovasc Surg*, vol. 36 Suppl 2, pp. 114-7, Jun 1988.

[6] B. L. Aronoff, "Review: Lasers: Reflections on their evolution," *Journal of Surgical Oncology*, vol. 64, no. 1, pp. 84-92, 1997. [Online]. Available:

[7] S. Stellar, T. G. Polanyi, and H. C. Bredemeier, "Lasers in surgery," in *Laser applications in medicine and biology*: Springer, 1974, pp. 241-293.

[8] S. Bown, "Phototherapy of tumors," *World journal of surgery*, vol. 7, no. 6, pp. 700-709, 1983.

[9] R. MUSCHTER and A. HOFSTETTER, "Interstitial laser therapy outcomes in benign prostatic hyperplasia," *Journal of endourology*, vol. 9, no. 2, pp. 129-135, 1995.

[10] Y. Huang, *Handbook of photomedicine*. CRC Press, 2013.

[11] A. Gupta and M. R. Hamblin, "History and fundamentals of low-level laser (light) therapy," in *Handbook of photomedicine*: CRC Press, 2013, pp. 67-78.

[12] Y. Feng, Z. Liu, and X.-S. Yi, "Co-occurrence of photochemical and thermal effects during laser polymer ablation via a 248-nm excimer laser," *Applied Surface Science*, vol. 156, no. 1-4, pp. 177-182, 2000.

[13] J. Estelrich and M. A. Busquets, "Iron Oxide Nanoparticles in Photothermal Therapy," *Molecules*, vol. 23, no. 7, p. 1567, 2018.

[14] C. P. Ruan *et al.*, "NIR-II light-modulated thermosensitive hydrogel for light-triggered cisplatin release and repeatable chemo-photothermal therapy," *Chemical Science,* vol. 10, no. 17, pp. 4699-4706, May 2019.

[15] D. Sordillo, L. Sordillo, P. Sordillo, and R. Alfano, *Fourth near-infrared optical window for assessment of bone and other tissues* (SPIE BiOS). SPIE, 2016.

[16] C.-C. Chen *et al.*, "DNA−Gold Nanorod Conjugates for Remote Control of Localized Gene Expression by near Infrared Irradiation," *Journal of the American Chemical Society,* vol. 128, no. 11, pp. 3709-3715, 2006/03/01 2006.

[17] G. L. Liu, J. Kim, Y. Lu, and L. P. Lee, "Optofluidic control using photothermal nanoparticles," *Nature Materials,* vol. 5, no. 1, pp. 27-32, 2006/01/01 2006.

[18] Y. Cai, Z. Wei, C. Song, C. Tang, W. Han, and X. Dong, "Optical nano-agents in the second near-infrared window for biomedical applications," *Chemical Society Reviews,* vol. 48, no. 1, pp. 22-37, 2019.

[19] B. Jean and T. Bende, "Mid-IR Laser Applications in Medicine," in *Solid-State Mid-Infrared Laser Sources,* I. T. Sorokina and K. L. Vodopyanov Eds. Berlin, Heidelberg: Springer Berlin Heidelberg, 2003, pp. 530-565.

[20] R. G. Calderhead, "Watts a joule: on the importance of accurate and correct reporting of laser parameters in low reactive-level laser therapy and photobioactivation research," *Laser Therapy,* vol. 3, no. 4, pp. 177-182, 1991.

[21] S. Sarkar *et al.*, "Cancer development, progression, and therapy: an epigenetic overview," *International journal of molecular sciences,* vol. 14, no. 10, pp. 21087-21113, 2013.

[22] M. J. Thun, E. E. Calle, C. Rodriguez, and P. A. Wingo, "Epidemiological research at the American cancer society," *Cancer Epidemiology and Prevention Biomarkers,* vol. 9, no. 9, pp. 861-868, 2000.

[23] R. L. Siegel, K. D. Miller, H. E. Fuchs, and A. Jemal, "Cancer Statistics, 2021," *CA: A Cancer Journal for Clinicians,* vol. 71, no. 1, pp. 7-33, 2021. [Online].

[24] J. C. Coffey, J. H. Wang, M. J. F. Smith, D. Bouchier-Hayes, T. G. Cotter, and H. P. Redmond, "Excisional surgery for cancer cure: therapy at a cost," *The Lancet Oncology,* vol. 4, no. 12, pp. 760-768, 2003/12/01/ 2003. [Online]..

[25] X. Hou, Y. Tao, Y. Pang, X. Li, G. Jiang, and Y. Liu, "Nanoparticle-based photothermal and photodynamic immunotherapy for tumor treatment," *International Journal of Cancer,* vol. 143, no. 12, pp. 3050-3060, 2018.

[26] S. W. Cramer and C. C. Chen, "Photodynamic Therapy for the Treatment of Glioblastoma," (in English), *Frontiers in Surgery,* Review vol. 6, no. 81, 2020-January-21 2020.

[27] A. P. Castano, T. N. Demidova, and M. R. Hamblin, "Mechanisms in photodynamic therapy: part one—photosensitizers, photochemistry and cellular localization," *Photodiagnosis and Photodynamic Therapy,* vol. 1, no. 4, pp. 279-293, 2004/12/01/ 2004.

[28] M. M. Kim and A. Darafsheh, "Light Sources and Dosimetry Techniques for Photodynamic Therapy," *Photochemistry and Photobiology,* vol. 96, no. 2, pp. 280-294, 2020.

[29] J. T. Walsh, "Basic interactions of light with tissue," in *Optical-thermal response of laser-irradiated tissue*: Springer, 2010, pp. 13-26.

[30] J. Chen *et al.*, "Nanomaterials as photothermal therapeutic agents," *Progress in Materials Science,* vol. 99, pp. 1-26, 2019/01/01/ 2019.

[31] C. J. DILLAHA, G. T. JANSEN, W. M. HONEYCUTT, and A. C. BRADFORD, "Selective Cytotoxic Effect of Topical 5-Fluorouracil," *Archives of Dermatology,* vol. 88, no. 3, pp. 247-256, 1963.

[32] F. Meyer-Betz, "Untersuchungen über die biologische (photodynamische) Wirkung des Hämatoporphyrins und anderer Derivate des Blut-und Gallenfarbstoffs," *Dtsch. Arch. Klin. Med,* vol. 112, no. 476-450, pp. 0366-8576, 1913.

[33] M. H. Gold and M. P. Goldman, "5-Aminolevulinic Acid Photodynamic Therapy: Where We Have Been and Where We Are Going," *Dermatologic Surgery,* vol. 30, no. 8, pp. 1077-1084, 2004.

[34] G. J. Hart, A. D. Miller, U. Beifuss, F. J. Leeper, and A. R. Battersby, "Biosynthesis of porphyrins and related macrocycles. Part 35. Discovery of a novel dipyrrolic cofactor essential for the catalytic action of hydroxymethylbilane synthase (porphobilinogen deaminase)," *Journal of the Chemical Society, Perkin Transactions 1,* no. 7, pp. 1979-1993, 1990.

[35] E. Epstein, "Fluorouracil paste treatment of thin basal cell carcinomas," *Archives of dermatology,* vol. 121, no. 2, pp. 207-213, 1985.

[36] E. Paszko, C. Ehrhardt, M. O. Senge, D. P. Kelleher, and J. V. Reynolds, "Nanodrug applications in photodynamic therapy," *Photodiagnosis and Photodynamic Therapy,* vol. 8, no. 1, pp. 14-29, 2011/03/01/ 2011.

[37] C. A. Robertson, D. H. Evans, and H. Abrahamse, "Photodynamic therapy (PDT): a short review on cellular mechanisms and cancer research applications for PDT," *Journal of Photochemistry and Photobiology B: Biology,* vol. 96, no. 1, pp. 1-8, 2009.

[38] A. Chicheł, J. Skowronek, M. Kubaszewska, and M. Kanikowski, "Hyperthermia – description of a method and a review of clinical applications," *Reports of Practical Oncology & Radiotherapy,* vol. 12, no. 5, pp. 267-275, 2007/09/01/ 2007.

[39] M. Hashemkhani, A. Muti, A. Sennaroğlu, and H. Yagci Acar, "Multimodal image-guided folic acid targeted Ag-based quantum dots for the combination of selective methotrexate delivery and photothermal therapy," *Journal of Photochemistry and Photobiology B: Biology,* vol. 213, p. 112082, 2020/12/01/ 2020.

[40] P. Sundaram and H. Abrahamse, "Phototherapy Combined with Carbon Nanomaterials (1D and 2D) and Their Applications in Cancer Therapy," *Materials,* vol. 13, no. 21, p. 4830, 2020.

[41] S. Nomura *et al.*, "Highly reliable, targeted photothermal cancer therapy combined with thermal dosimetry using a near-infrared absorbent," *Scientific Reports,* vol. 10, no. 1, p. 9765, 2020/06/17 2020.

[42] J. Stabile *et al.*, "Chapter 12 - Engineering gold nanoparticles for photothermal therapy, surgery, and imaging," in *Nanoparticles for Biomedical Applications*, E. J. Chung, L. Leon, and C. Rinaldi Eds.: Elsevier, 2020, pp. 175-193.

[43] R. Hanf, S. Fey, M. Schmitt, G. Hermann, B. Dietzek, and J. Popp, "Catalytic efficiency of a photoenzyme—an adaptation to natural light conditions," *ChemPhysChem,* vol. 13, no. 8, pp. 2013-2015, 2012.

[44] J. T. Robinson *et al.*, "High performance in vivo near-IR (> 1 μm) imaging and photothermal cancer therapy with carbon nanotubes," *Nano research,* vol. 3, no. 11, pp. 779-793, 2010.

[45] L. O. Svaasand, C. J. Gomer, and E. Morinelli, "On the physical rationale of laser induced hyperthermia," *Lasers in Medical Science,* vol. 5, no. 2, pp. 121-128, 1990/06/01 1990.

[46] X. He, W. F. Wolkers, J. H. Crowe, D. J. Swanlund, and J. C. Bischof, "In Situ Thermal Denaturation of Proteins in Dunning AT-1 Prostate Cancer Cells: Implication for Hyperthermic Cell Injury," *Annals of Biomedical Engineering,* vol. 32, no. 10, pp. 1384-1398, 2004/10/01 2004..

[47] J. R. Melamed, R. S. Edelstein, and E. S. Day, "Elucidating the Fundamental Mechanisms of Cell Death Triggered by Photothermal Therapy," *ACS Nano,* vol. 9, no. 1, pp. 6-11, 2015/01/27 2015.

[48] K. Bilici *et al.*, "Broad spectrum antibacterial photodynamic and photothermal therapy achieved with indocyanine green loaded SPIONs under near infrared irradiation," *Biomaterials Science,* 10.1039/D0BM00821D vol. 8, no. 16, pp. 4616-4625, 2020.

[49] M. Ramasamy, S. S. Lee, D. K. Yi, and K. Kim, "Magnetic, optical gold nanorods for recyclable photothermal ablation of bacteria," *Journal of Materials Chemistry B,* 10.1039/C3TB21310B vol. 2, no. 8, pp. 981-988, 2014.

[50] H. Chen *et al.*, "Understanding the Photothermal Conversion Efficiency of Gold Nanocrystals," *Small,* vol. 6, no. 20, pp. 2272-2280, 2010.

[51] T. Park *et al.*, "ICG-loaded PEGylated BSA-silver nanoparticles for effective photothermal cancer therapy," *International Journal of Nanomedicine,* vol. 15, p. 5459, 2020.

[52] M. Hashemkhani, K. Bilici, A. Muti, A. Sennaroglu, and H. Y. Acar, "Ag2S-Glutathione quantum dots for NIR image guided photothermal therapy," *New Journal of Chemistry,* 10.1039/C9NJ04608A vol. 44, no. 14, pp. 5419-5427, 2020.

[53] A. R. Burke *et al.*, "The resistance of breast cancer stem cells to conventional hyperthermia and their sensitivity to nanoparticle-mediated photothermal therapy," *Biomaterials,* vol. 33, no. 10, pp. 2961-2970, 2012/04/01/ 2012.

[54] C. Hong, J. Lee, H. Zheng, S.-S. Hong, and C. Lee, "Porous silicon nanoparticles for cancer photothermotherapy," *Nanoscale Research Letters,* vol. 6, no. 1, p. 321, 2011/04/11 2011.

[55] W. Liu, X. Zhang, L. Zhou, L. Shang, and Z. Su, "Reduced graphene oxide (rGO) hybridized hydrogel as a near-infrared (NIR)/pH dual-responsive platform for combined chemo-photothermal therapy," *Journal of Colloid and Interface Science,* vol. 536, pp. 160-170, 2019/02/15/ 2019.

[56] K. Bilici, A. Muti, A. Sennaroğlu, and H. Yagci Acar, "Indocyanine green loaded APTMS coated SPIONs for dual phototherapy of cancer," *Journal of Photochemistry and Photobiology B: Biology,* vol. 201, p. 111648, 2019/12/01/ 2019.

[57] K. Bilici, A. Muti, F. Demir Duman, A. Sennaroğlu, and H. Yağcı Acar, "Investigation of the factors affecting the photothermal therapy potential of small iron oxide nanoparticles over the 730–840 nm spectral region," *Photochemical & Photobiological Sciences,* 10.1039/C8PP00203G vol. 17, no. 11, pp. 1787-1793, 2018.

[58] T. Yang *et al.*, "Size-Dependent Ag2S Nanodots for Second Near-Infrared Fluorescence/Photoacoustics Imaging and Simultaneous Photothermal Therapy," *ACS Nano,* vol. 11, no. 2, pp. 1848-1857, 2017/02/28 2017, doi: 10.1021/acsnano.6b07866.

[59] L. Dong *et al.*, "Multifunctional Cu–Ag2S nanoparticles with high photothermal conversion efficiency for photoacoustic imaging-guided photothermal therapy in vivo," *Nanoscale,* 10.1039/C7NR07263E vol. 10, no. 2, pp. 825-831, 2018.

[60] D. K. Roper, W. Ahn, and M. Hoepfner, "Microscale Heat Transfer Transduced by Surface Plasmon Resonant Gold Nanoparticles," *The Journal of Physical Chemistry C,* vol. 111, no. 9, pp. 3636-3641, 2007/03/01 2007.

[61] J. Gao, C. Wu, D. Deng, P. Wu, and C. Cai, "Direct Synthesis of Water-Soluble Aptamer-Ag2S Quantum Dots at Ambient Temperature for Specific Imaging and Photothermal Therapy of Cancer," *Advanced Healthcare Materials,* vol. 5, no. 18, pp. 2437-2449, 2016.

[62] J. Yang, R.-X. Xia, M.-H. Yao, R.-M. Jin, Y.-D. Zhao, and B. Liu, "High quantum yield $Ag_2S$ quantum dot@ polypeptide-engineered hybrid nanogels for targeted second near-infrared fluorescence/photoacoustic imaging and photothermal therapy," 2018.

[63] W. C. Dewey, "Arrhenius relationships from the molecule and cell to the clinic," *International Journal of Hyperthermia,* vol. 10, no. 4, pp. 457-483, 1994/01/01 1994.

[64] P. Wust *et al.*, "Hyperthermia in combined treatment of cancer," *The Lancet Oncology,* vol. 3, no. 8, pp. 487-497, 2002/08/01/ 2002.

[65] D. T. Phan, T. T. V. Phan, N. T. Bui, S. Park, J. Choi, and J. Oh, "A portable device with low-power consumption for monitoring mouse vital signs during in vivo photoacoustic imaging and photothermal therapy," *Physiological Measurement,* vol. 41, no. 12, p. 125011, 2020.

[66] C. J. Gordon, "The mouse thermoregulatory system: Its impact on translating biomedical data to humans," *Physiology & behavior,* vol. 179, pp. 55-66, 2017.

[67] P. W. B. R. C. H. J. G. P. S. V. B. R. F. W. Tilly, "Temperature data and specific absorption rates in pelvic tumours: predictive factors and correlations," *International Journal of Hyperthermia,* vol. 17, no. 2, pp. 172-188, 2001/01/01 2001.

[68] M. G. Skinner, M. N. Iizuka, M. C. Kolios, and M. D. Sherar, "A theoretical comparison of energy sources-microwave, ultrasound and laser-for interstitial thermal therapy," *Physics in Medicine & Biology,* vol. 43, no. 12, p. 3535, 1998.

[69] L. Peltonen and V. A. McKusick, "Genomics and medicine. Dissecting human disease in the postgenomic era," (in eng), *Science,* vol. 291, no. 5507, pp. 1224-9, Feb 16 2001.

[70] J. Speakman, "Measuring Energy Metabolism in the Mouse – Theoretical, Practical, and Analytical Considerations," (in English), *Frontiers in Physiology,* Review vol. 4, 2013-March-14 2013.

[71] C. J. Gordon, "Quantifying the instability of core temperature in rodents," *Journal of Thermal Biology,* vol. 34, no. 5, pp. 213-219, 2009.

[72] D. S. Ramsay and S. C. Woods, "Clarifying the roles of homeostasis and allostasis in physiological regulation," *Psychological review,* vol. 121, no. 2, p. 225, 2014.

[73] A. L. B. P. Andrei P. Sommer, Adam R. Mester, Ralf-Peter Franke, and Harry T. Whelan, "Biostimulatory Windows in Low-Intensity Laser Activation: Lasers, Scanners, and NASA's Light-Emitting Diode Array System," *Journal of Clinical Laser Medicine & Surgery,* vol. 19, no. 1, pp. 29-33, 2001.

[74] V. Mulens-Arias *et al.*, "Tumor-Selective Immune-Active Mild Hyperthermia Associated with Chemotherapy in Colon Peritoneal Metastasis by Photoactivation of Fluorouracil-Gold Nanoparticle Complexes," (in eng), *ACS Nano,* vol. 15, no. 2, pp. 3330-3348, Feb 23 2021.

[75] G.-G. Yang, Z.-Y. Pan, D.-Y. Zhang, Q. Cao, L.-N. Ji, and Z.-W. Mao, "Precisely Assembled Nanoparticles against Cisplatin Resistance via Cancer-Specific Targeting of Mitochondria and Imaging-Guided Chemo-Photothermal Therapy," *ACS Applied Materials & Interfaces,* vol. 12, no. 39, pp. 43444-43455, 2020/09/30 2020, doi: 10.1021/acsami.0c12814.

[76] G. Cui, P. He, L. Yu, C. Wen, X. Xie, and G. Yao, "Oxygen self-enriched nanoplatform combined with US imaging and chemo/photothermal therapy for breast cancer," *Nanomedicine: Nanotechnology, Biology and Medicine,* vol. 29, p. 102238, 2020/10/01/ 2020..

[77] V. Shanmugam *et al.*, "Oligonucleotides—Assembled Au Nanorod-Assisted Cancer Photothermal Ablation and Combination Chemotherapy with Targeted Dual-Drug Delivery of Doxorubicin and Cisplatin Prodrug," *ACS Applied Materials & Interfaces,* vol. 6, no. 6, pp. 4382-4393, 2014/03/26 2014.

[78] H. Sung *et al.*, "Global Cancer Statistics 2020: GLOBOCAN Estimates of Incidence and Mortality Worldwide for 36 Cancers in 185 Countries," *CA: A Cancer Journal for Clinicians,* vol. 71, no. 3, pp. 209-249, 2021.

[79] F. M. Kievit and M. Zhang, "Surface Engineering of Iron Oxide Nanoparticles for Targeted Cancer Therapy," *Accounts of Chemical Research,* vol. 44, no. 10, pp. 853-862, 2011/10/18 2011.

[80] A. Vogel and V. Venugopalan, "Mechanisms of Pulsed Laser Ablation of Biological Tissues," *Chemical Reviews,* vol. 103, no. 2, pp. 577-644, 2003/02/01 2003, doi: 10.1021/cr010379n.

[81] C. P. Nolsøe *et al.*, "Interstitial hyperthermia of colorectal liver metastases with a US-guided Nd-YAG laser with a diffuser tip: a pilot clinical study," *Radiology,* vol. 187, no. 2, pp. 333-337, 1993.

[82] S. K. Chinnadurai, J. G. Johnson Iii, and J. N. Langan, "Comparison of 3 Methods for Preventing Perianesthetic Hypothermia in Callimicos (Callimico goeldii)," *Journal of the American Association for Laboratory Animal Science,* vol. 56, no. 3, pp. 318-321, // 2017.

[83] A. Sennaroğlu, *Photonics and Laser Engineering: Principles, Devices, and Applications*. McGraw Hill, 2010.

[84] B. A. B. a. J. H. Weiner, *Theory of Thermal Stresses*. Dover Publication, 1997.